Neuropilin-1 controls vascular permeability through juxtacrine regulation of endothelial adherens junctions

Sagnik Pal, Yangyang Su, Lena Claesson-Welsh, and Mark Richards*

Dept. of Immunology, Genetics and Pathology, Beijer and Science for Life Laboratories, Uppsala University, Uppsala, Sweden

*) Corresponding author at the address above or mark.richards@igp.uu.se

Key words: Neuropilin 1, vascular permeability, signalling, VE-cadherin, VEGF

Abstract

Neuropilin-1 (NRP1) regulates endothelial cell (EC) biology through modulating vascular endothelial growth factor receptor 2 (VEGFR2) signalling by presenting VEGFA. How NRP1 impacts VEGFA-mediated vascular hyperpermeability however is unresolved, being described as having a positive or passive function. Using EC-specific *Nrp1* knock-out mice, we discover that EC-expressed NRP1 exerts an organotypic role. In ear skin, VEGFA/VEGFR2-mediated vascular leakage increased following EC NRP1 knock-out, showing that NRP1 negatively regulates VEGFR2 signalling. Conversely, in back skin and trachea, EC NRP1 knock-out decreased vascular leakage. Accordingly, VE-cadherin phosphorylation increased in the ear skin but was suppressed in back skin of *Nrp1* iECKO mice. NRP1 has been shown to have the ability to act in a juxtacrine manner. Importantly, NRP1 was more abundant in perivascular cells of the ear skin than back skin. Global NRP1 knock-out suppressed VEGFA-induced vascular leakage in the ear skin, implicating perivascular NRP1 as a juxtacrine co-receptor of VEGFA in this compartment. Altogether, we demonstrate that perivascular NRP1 is an active participant in EC VEGFA/VEGFR2 signalling and acts as an organotypic modifier of EC biology.

Introduction

Neuropilin 1 (NRP1) is a multifunctional transmembrane protein that is expressed abundantly on the surface of a range cell types, where it binds class 3 semaphorins (SEMA3), heparan sulfate and vascular endothelial growth factors (VEGFs) (Goshima et al., 1999, Mamluk et al., 2002, Gu et al., 2002). VEGFA is the main activator of VEGF receptor 2 (VEGFR2) signalling in endothelial cells (ECs) and its binding to NRP1 promotes heterocomplex formation between NRP1 and VEGFR2 (Soker et al., 2002). Thus, NRP1 has been designated as a co-receptor of VEGFR2 and is known to modulate VEGFR2 signalling. The cytoplasmic domain of NRP1 contains a C-terminal SEA motif, a PDZ binding domain that mediates binding to synectin (GIPC1) and in-turn regulates the endocytic trafficking of both NRP1 and VEGFR2 (Cai and Reed, 1999, Naccache et al., 2006, Horowitz and Seerapu, 2012, Lanahan et al., 2010). Accordingly, removal of the NRP1 cytoplasmic tail delays VEGFR2 endocytosis following VEGFA binding, leading to enhanced surface retention and reduced phosphorylation of tyrosine (Y)1175 in VEGFR2 (Lanahan et al., 2013). NRP1 thus acts as an important modulator of VEGFR2 activation and its downstream signalling pathways. However, reports have also suggested that VEGFA transduces biological responses in ECs via NRP1, in a VEGFR2-independent manner (Roth et al., 2016).

Global NRP1 knockout in mice results in lethality at E10-E12.5 due to abnormal vessel sprouting in major organs and impaired yolk sac vascularization (Kawasaki et al., 1999). Moreover, NRP1 overexpression leads to excessive vessel growth and promotes leaky and haemorrhagic vessels (Kitsukawa et al., 1995). Endothelial-specific knockout of NRP1 in mouse embryos only show mild embryonic brain defects, while in the adult vasculature no gross abnormalities are evident (Lanahan et al., 2013). Several reports also link increased NRP1 expression in tumours to a poor prognosis for survival (Miao et al., 2000, Kawakami et al., 2002, Hong et al., 2007). Furthermore, in diseases such as age related macular degeneration, NRP1 has been linked with increased neovascularization and vessel hyperpermeability, likely due to enhanced signalling downstream of VEGFA (Raimondi et al., 2014, Fernández-Robredo et al., 2017).

VEGFA-induced vascular permeability is mediated through the Y949 and Y1173 phosphosites of VEGFR2. The phosphorylated Y949 presents a binding site for TSAd (T-cell specific adaptor), which in turn binds SFKs (Src family kinases) that phosphorylate and promote internalization of junctional proteins such as VE-cadherin (Matsumoto et al., 2005, Sun et al., 2012, Li et al., 2016, Jin et al., 2022). Concurrently, pY1173 phosphorylates PLCϒ, leading to Ca2+/Protein kinase C (PKC) activation of endothelial nitric oxide synthase (eNOS), contributing to Src activation and phosphorylation of VE-cadherin (Sjoberg et al., 2023). The role of NRP1 in VEGFA-mediated permeability has been controversial. Studies employing *in* vivo and *in vitro* models have found NRP1 to be a positive regulator of VEGFA-mediated vascular permeability, or to lack effect, dependent on tissue or

63 experimental setup (Fantin et al., 2017, Acevedo et al., 2008, Wang et al., 2015, Becker et al., 2005,
64 Pan et al., 2007, Cerani et al., 2013). Additionally, treatment of ECs with CendR peptides, which bind
65 and induce internalisation of NRP1, increases permeability in a NRP1-dependent, but VEGFR2-
66 independent manner (Roth et al., 2016). Therefore, the exact role of NRP1 in VEGFA-VEGFR2
67 mediated permeability remains unclear. NRP1 is a promising target in a number of pathologies where
68 vascular dysfunction is exacerbative. Understanding the relationship between NRP1 and VEGFA-
69 VEGFR2 signalling is thus of potential therapeutic benefit.

70 Here, we aimed to further uncover the role of NRP1 in VEGFA-mediated vascular permeability. Using
71 mice with global or EC-specific loss of NRP1 expression, we identify a tissue-specific role for
72 endothelial NRP1 in the modulation of VEGFA/VEGFR2 signalling regulating vascular leakage. We find
73 that endothelial-specific loss of NRP1 (*Nrp1* iECKO) can both increase and decrease VEGFA-mediated
74 vascular leakage, dependent on the vascular bed. NRP1 is widely expressed and is an important
75 constituent of peri-vascular cells in some, but not all, tissues and vessel subtypes. The consequence
76 of global loss of NRP1 expression demonstrates that peri-vascular NRP1 can modify VEGFA/VEGFR2-
77 induced vascular leakage and steer the tissue-specific role of endothelial NRP1 in barrier integrity.
78 Collectively, these data reveal that the relative expression levels of NRP1 between perivascular cells
79 and ECs acts as a tissue-specific modifier of EC VEGFA/VEGFR2 signalling upstream of vascular
80 leakage.

81

82 **Results**

83 <u>NRP1 regulates VEGFA-mediated permeability in an organotypic manner</u>

84 NRP1 has been studied extensively as a co-receptor of the VEGFA/VEGFR2 pathway, and its ability to
85 modulate VEGFR2 signalling in developmental and pathological angiogenesis has been clearly
86 established. However, results concerning the role of NRP1 in VEGFA-mediated vascular permeability
87 have remained contradictory (Fantin et al., 2017, Acevedo et al., 2008, Wang et al., 2015, Becker et
88 al., 2005, Pan et al., 2007, Cerani et al., 2013). *Nrp1*$^{fl/fl}$; *Cdh5*^{CreERT2} (*Nrp1* iECKO) mice were used to
89 study the EC-specific role of NRP1 in VEGFA-induced vascular leakage. Following tamoxifen
90 administration, a 75% reduction in NRP1 protein levels was achieved in lung tissue, chosen for
91 analysis due to the high EC content (Figure 1A and B). Furthermore, using immunofluorescent
92 stainings, reduction in NRP1 levels could be observed in the ear and back skin vascular beds with the
93 loss of EC NRP1 (Supp. figure 1A and B). Using a highly sensitive assay combining intravital
94 microscopy and atraumatic intradermal microinjection in the ear skin of *Nrp1* iECKO mice, VEGFA-
95 induced vascular leakage was significantly increased following the loss of NRP1 (Figure 1C and D)

96 (Honkura et al., 2018). Additionally, we measured qualitative aspects of vascular leakage including lag
97 period (time from stimulation to leakage onset) and degree of leakage (rate of dextran
98 extravasation). These analyses showed that ECs in *Nrp1* iECKO mice respond faster to stimulation
99 (Figure 1E) and exhibit more profuse leakage at each site (Figure 1F), indicative of increased
100 disruption of EC-EC junctions. These data suggest that NRP1 exerts a stabilizing role by suppressing
101 VEGFA-induced endothelial junction disruption in the ear dermis. This finding is in contrast to reports
102 showing NRP1 to be a positive regulator of VEGFA-mediated vascular leakage (Fantin et al., 2017,
103 Acevedo et al., 2008, Becker et al., 2005).

104 One possible explanation for these differences compared to previous reports is that the role of NRP1
105 may be organ dependent, in line with the growing insights into the distinct properties of ECs in
106 different vessel types and vascular beds (Augustin and Koh, 2017). To investigate a potential
107 organotypic role for NRP1 in EC biology, we studied the consequence of *Nrp1* knockout on the barrier
108 properties of ECs in different vascular beds.

109 Initially, selected organs, chosen based on prior experience of their different EC barrier properties
110 (Aird, 2007, Augustin and Koh, 2017, Richards et al., 2022), were investigated for their susceptibility
111 to VEGFA-induced vascular leakage via the systemic administration of fluorescent dextrans with or
112 without VEGFA. After 30 minutes, organs were collected and acute vascular leakage assessed
113 microscopically or following solvent-based extraction of dextran and fluorescence spectroscopy. All
114 organs analysed, except for the liver, showed vascular leakage after VEGFA stimulation (Supp. figure
115 2A - E). The role of endothelial NRP1 in these organs was further studied in *Nrp1* iECKO mice,
116 showing significantly decreased VEGFA-mediated vascular leakage in the trachea and back skin
117 (Figure 1G and H, Supp. figure 3). Kidney, skeletal muscle and heart in contrast did not show a
118 significant difference in VEGFA-mediated vascular leakage following the loss of EC-expressed NRP1
119 (Figure 1I and J).

120 These data collectively suggest that endothelial NRP1 has an organ-specific role in controlling VEGFA-
121 mediated vascular permeability. Importantly, endothelial NRP1 is a positive regulator of VEGFA
122 mediated permeability in the trachea and back skin but a negative regulator in the ear skin.

123

124 <u>Global inactivation of NRP1 reduces VEGFA-mediated vascular permeability</u>

125 Our results here, where NRP1 may play positive (trachea and back skin), negative (ear skin) and
126 passive (kidney, skeletal muscle and heart) role in VEGFA-induced vascular leakage, were collected
127 using EC-specific knockout mice. In previous studies, mouse models of both EC-specific deletion and a

128 globally expressed NRP1 C-terminal deletion mutant were employed (Fantin et al., 2017, Roth et al.,
129 2016). We thus set out to investigate whether global inactivation of NRP1 using an anti-NRP1
130 blocking antibody might differently modify the VEGFA-induced leakage response. Wild-type C57Bl/6
131 mice were locally treated in the ear dermis with an anti-NRP1 antibody via intradermal injection,
132 followed by intravital assessment of VEGFA-induced vascular permeability. Interestingly, NRP1
133 blockade reduced vascular leakage in the ear dermis when compared to isotype control (Supp. figure
134 4A). This is in contrast to the EC-specific loss of NRP1 in *Nrp1* iECKO mice, which resulted in enhanced
135 VEGFA-mediated vascular leakage (Figure 1C-F). We similarly investigated the effect of blocking NRP1
136 on the back skin and tracheal vasculatures. Treatment with anti-NRP1 antibody was found to reduce
137 VEGFA-induced leakage in both tissues following local and systemic administration of VEGFA
138 respectively (Supp. figure 4B and C).

139 To verify the findings using neutralizing anti-NRP1 antibodies, we crossed $Nrp1^{fl/fl}$ with $Actb^{CreERT}$ mice
140 to generate global *Nrp1* knock-out mice (*Nrp1* iKO). Efficient reduction of NRP1 protein was
141 confirmed in lung lysates (Figure 2A and B). Complete loss of NRP1 could also be seen in the ear and
142 back skin of these mice using immunofluorescent staining (Supp. figure 1). Intravital imaging of the
143 ear dermis of *Nrp1* iKO mice showed that global loss of NRP1 reduced VEGFA-induced vascular
144 leakage, in contrast to the phenotype seen in *Nrp1* iECKO mouse ear skin and in agreement with
145 blocking antibody data (Figure 2C and D). Furthermore, global *Nrp1* knock-out resulted in a ~75%
146 reduction in VEGFA-mediated vascular leakage also in the back skin and tracheal vasculatures, similar
147 to that seen in *Nrp1* iECKO mice (Figure 2E and F).

148 These data illustrate the heterogenous nature of EC signalling regulation in different vascular beds,
149 and show that NRP1 modulates VEGFA signaling in an organotypic and cell-specific manner. Notably,
150 we demonstrate that VEGFA-induced leakage in the back skin and trachea is indistinguishable
151 between endothelial-specific and global *Nrp1* KO mice, whereas in the ear skin there is a contrasting
152 phenotype.

153

154 <u>NRP1 is heterogeneously expressed in perivascular cells</u>

155 NRP1 is known to form a heterocomplex with VEGFR2 upon VEGFA binding. Interestingly,
156 VEGFR2/NRP1/VEGFA can assemble as a juxtacrine *trans* complex, where NRP1 and VEGFR2 are
157 expressed on the surface of adjacent cells, as well as a *cis* complex, where NRP1 and VEGFR2 are
158 expressed on the same cell (Koch et al., 2014). Importantly, even though the kinetics of *trans*
159 VEGFR2/NRP1 complex formation is slow, these complexes are stable and produce a distinct
160 signalling output compared to the *cis* configuration (Koch et al., 2014). Thus, NRP1 presented in *cis* or

161 *trans* produces differential VEGFR2 signalling output upon VEGFA binding. Given the above findings
162 we reasoned that peri-endothelial distribution of NRP1 could be an important modifier of EC VEGFR2
163 signalling and possibly explain organotypic differences observed in *Nrp1* iECKO mice.

164 To investigate the pattern of NRP1 expression we employed a *Pdgfrβ* promoter-driven GFP (*Pdgfrβ-*
165 *GFP*) mouse to visualize PDGFRβ-positive pericytes. To visualize ECs, and the localization of NRP1 in
166 the ear skin and back skin from these mice, tissues were immunostained for CD31 and NRP1,
167 respectively. NRP1 expression could be seen in both endothelial and perivascular cells, which was
168 lost after global *Nrp1* deletion (Figure 3A and Supp. Figure 1). Both arteriolar (Figure 3B) and capillary
169 (Figure 3C) PDGFRβ-positive perivascular cells expressed NRP1. The relative level of perivascular/EC
170 expression of NRP1 was higher in the ear skin compared to back skin. In venules, the low expression
171 of NRP1 in perivascular cells in the back skin resulted in a 5-fold difference in the perivascular/EC
172 NRP1 ratio, when comparing the ear skin to back skin (Figure 3D).

173 These data thus show that NRP1 is expressed in perivascular cells of the ear skin and back skin. We
174 find however that the ratio of NRP1 expression between ECs and perivascular cells differs between
175 ear skin and back skin, and between different vessel types. In ear skin the perivascular/EC ratio is
176 higher compared to the back skin, which may support a higher ratio of *trans* NRP1/VEGFR2 relative
177 to cis complexes in the ear skin.

178

179 <u>NRP1 distribution modifies VEGFA-mediated signalling and vascular leakage</u>

180 NRP1 modifies VEGFR2 signalling by controlling its internalisation and intracellular trafficking (Bayliss
181 et al., 2020, Ballmer-Hofer et al., 2011). The presence of NRP1 in *trans* however, modifies this
182 dynamic and retains VEGFR2 at the cell surface for longer time periods, altering its signalling output
183 (Koch et al., 2014).

184 We thus wished to investigate whether perivascular NRP1 expression might interact with and alter
185 VEGFR2 signalling upstream of vascular leakage, and explain the above described organotypic effects
186 of EC NRP1 loss. For this purpose, *Nrp1* iECKO mice were crossed with homozygous *Vegfr2*$^{Y949F/Y949F}$
187 mice, to produce *Vegfr2*$^{Y949F/Y949F}$;*Nrp1* iECKO mice that are deficient in both EC NRP1 expression and
188 VEGFA-mediated vascular leakage ability. In these mice, loss of NRP1 protein was efficiently
189 established in lung tissue (Figure 4A and B). Analysis of VEGFA-mediated vascular leakage in the ear
190 dermis showed that the increased leakage, induced by the loss of EC NRP1, was abrogated by the loss
191 of the VEGFR2 phosphosite Y949, known to be required for activation of Src in response to VEGFA

192 (Figure 4C and D). These analyses suggest that, in the ear dermis, EC NRP1 negatively regulates
193 VEGFA-induced vascular leakage by modulation of VEGFR2 activation and phosphorylation.

194 We next sought to determine the relationship between NRP1 and VEGFR2 Y949 signalling in the
195 trachea and back skin vasculatures. Leakage in *Vegfr2*$^{Y949F/Y949F}$;*Nrp1* iECKO mice was induced by
196 systemic VEGFA and fluorescent 2000 kDa dextran administration in both *Nrp1* iECKO and
197 *Vegfr2*$^{Y949F/Y949F}$;*Nrp1* iECKO mice. As we observed previously, loss of EC NRP1 reduced vascular
198 leakage in the trachea and back skin by 75%, an effect that was enhanced further by the VEGFR2
199 Y949F mutation (Figure 4E and F). Importantly, leakage was similarly inhibited in the *Vegfr2*$^{Y949F/Y949F}$
200 model as in the combined *Vegfr2*$^{Y949F/Y949F}$;*Nrp1* iECKO mice in both the trachea and back skin. These
201 data show that NRP1 presented in *trans* by perivascular cells in the ear dermis can signal through
202 VEGFR2 to induce vascular leakage, and that VEGFR2 Y949 is vital for mediating NRP1's effects on
203 endothelial junctions.

204

205 <u>Perivascular NRP1 modifies VEGFA-induced signalling</u>

206 VEGFA/VEGFR2 signalling mediates phosphorylation of VE-Cadherin on Y685, required for vascular
207 permeability (Orsenigo et al., 2012, Wessel et al., 2014). We have also recently shown that PLCγ is an
208 important mediator of VEGFA-induced vascular leakage by allowing the production of nitric oxide
209 through eNOS, which in turn modified Src by tyrosine nitration, required for full Src activity (Sjoberg
210 et al., 2023). To clarify the impact of perivascular NRP1 on VEGFA-induced signalling we studied VE-
211 Cadherin and PLCγ phosphorylation in *Nrp1* iECKO and *Nrp1* iKO mice (Figure 5). Perivascular NRP1
212 expression in the ear dermis of *Nrp1* iECKO mice was lost in *Nrp1* iKO mice (Supp. figure 1). In
213 agreement with the enhanced vascular leakage in the ear dermis of *Nrp1* iECKO mice, VE-Cadherin
214 phosphorylation at Y685 was enhanced following intradermal VEGFA injection (Figure 5A). No such
215 induction was seen in *Nrp1* iKO mice (Figure 5B). In the back skin, VE-Cadherin pY685 levels were
216 induced by VEGFA in the control but not in the *Nrp1* iECKO, nor the iKO models (Figure 5C and D), in
217 accordance with the permeability phenotype (see Figure 1). Similarly, PLCγ phosphorylation was
218 potentiated in the ear skin of *Nrp1* iECKO but not *Nrp1* iKO mice (Supp. figure 5A and B). Moreover,
219 in the back skin loss of either endothelial or global NRP1 led to a reduction in PLCγ phosphorylation
220 following intradermal VEGFA stimulation (Supp. figure 5C and D).

221 Taken together these data show that NRP1 is expressed by perivascular cells in a tissue-specific
222 manner and that perivascular NRP1 can be an important modulator of VEGFA-signalling. In the ear
223 dermis, NRP1 is expressed by both endothelial and perivascular cells, forming *cis* and *trans*
224 interactions with VEGFR2 respectively. Whilst the *cis* EC interaction predominates, loss of EC NRP1

225 promotes *trans* NRP1/VEGFR2 interaction and potentiates VEGFA-induced signalling regulating
226 vascular leakage (Figure 6). Meanwhile, due to a paucity of perivascular NRP1 in the trachea and back
227 skin vasculatures, loss of EC NRP1 leads to a loss of NRP1:VEGFR2 complexes, attenuating VEGFA-
228 regulated vascular leakage.

229

230 **Discussion**

231 Here we find that NRP1 expression by perivascular cells is an important modulator of
232 VEGFA signalling regulating endothelial junction stability. Our data suggest that NRP1 presented in a
233 juxtacrine manner can potentiate certain VEGFR2 signalling upstream of vascular leakage. NRP1 is
234 expressed by a number of cells adjacent to blood vessels, including PDGFRβ-positive pericytes.
235 However, the abundance of these cells and their level of NRP1 expression differ between vascular
236 beds. Loss of EC-specific NRP1 thus has a differential effect on VEGFA-mediated vascular leakage in
237 different vascular beds, dependent on the ability of ECs to form *tran*s NRP1/VEGFR2 complexes.

238 Numerous studies have implicated endothelial NRP1 as a positive regulator of
239 permeability (Fantin et al., 2017, Becker et al., 2005, Acevedo et al., 2008). However, multiple studies
240 argue against this, with NRP1 blockade or deletion having no effect on VEGFA-induced vascular
241 leakage in the skin and retina (Pan et al., 2007, Cerani et al., 2013). Here we find that the function of
242 endothelial NRP1 in VEGFA-mediated vascular permeability varies in different vascular beds. In
243 keeping with previous data, we find that loss of NRP1 reduces VEGFA-induced vascular leakage in the
244 back skin and trachea. Meanwhile, endothelial NRP1 appears to have no effect on VEGFA-induced
245 vascular leakage in kidney, skeletal muscle and heart. In the ear skin, however, loss of NRP1
246 surprisingly leads to an increase in VEGFA-induced vascular leakage. This appears to be through
247 enhanced VEGFR2 Y949 signalling, as mutation of this phosphosite normalises the enhanced leakage
248 seen after loss of NRP1. Previous publications have described NRP1 as being pivotal for VEGFR2-
249 induced Src activity via recruitment of Abl kinase (Fantin et al., 2017). How exactly VEGFA-VEGFR2
250 signals to Abl, and whether this requires the Y949 phosphosite, however is unknown. Further work is
251 required to understand exactly how NRP1 modifies VEGFR2 activity and how this differs between
252 different vascular beds.

253 As others have noted and we see here, NRP1 is expressed by perivascular cells,
254 including PDGFRβ positive pericytes (Bartlett et al., 2017, Wnuk et al., 2017). However, we find that
255 perivascular NRP1 expression and its ratio to EC expression differs between different vascular beds,
256 being higher in the ear skin than back skin. When the *trans* NRP1/VEGFR2 complex predominates, as
257 in the ear skin of *Nrp1* iECKO mice, our data indicate that VEGFA/VEGFR2 signalling impacting

258 junction stability is potentiated. This is in keeping with reports showing that NRP1 presented in *trans*
259 can modify VEGFR2 signalling kinetics, resulting in prolonged PLCγ and ERK2 phosphorylation (Koch
260 et al., 2014). However how such prolonged kinetics might affect the VEGFR2 signalling pathways
261 upstream of vascular leakage has not been previously explored. In addition, juxtacrine NRP1
262 interactions have been shown to have important functions in cell types other than ECs. For example,
263 NRP1 expressed on microglia is important for the trans-activation of PDGFRα on oligodendrocyte
264 precursor cells, resulting in enhanced proliferation and myelin repair (Sherafat et al., 2021).
265 Furthermore, NRP1 has been posited as a potential immune checkpoint inhibitor (Sarris et al., 2008).
266 NRP1 is highly expressed by regulatory T cells, as well as antigen presenting dendritic cells, and the
267 formation of *tran*s NRP1 homodimers has been suggested to stabilise regulatory T cell function and
268 promote immune tolerance. Finally, numerous studies have described the expression of NRP1 on
269 tumour cells, which can modify EC behaviour and alter their angiogenic potential (Koch et al., 2014,
270 Miao et al., 2000, Hu et al., 2007, Shahrabi-Farahani et al., 2016). This may partly be due to the ability
271 of NRP1 to bind VEGFA and thus provide a pool of tumoural VEGFA towards which ECs migrate. In
272 tumours, NRP1 can also form juxtacrine interactions with VEGFR2 on ECs upon VEFGA binding and
273 modify intracellular EC signalling compared to NRP1 action in a *cis* manner (Koch et al., 2014, Morin
274 et al., 2020, Morin et al., 2018).

275 One possible mechanism by which NRP1 presented in *trans* might alter
276 VEGFA/VEGFR2 signalling, when compared to *cis*, is via modification of VEGFR2 trafficking. The
277 adapter molecule synectin is an important intracellular binding partner of NRP1 and facilitates
278 myosin IV-mediated endocytosis (Cai and Reed, 1999, Naccache et al., 2006). A recent study also
279 found that NRP1 interacts with members of the ERM family of intracellular proteins, which act as
280 intermediaries between the plasma membrane and actin cytoskeleton and that have also been
281 associated with endocytosis and intracellular trafficking (Ponuwei, 2016, Gioelli et al., 2022). NRP1
282 may thus function not just as a co-receptor, but also as a linker to mediate the intracellular trafficking
283 of cell surface receptors. This idea is supported by studies showing that NRP1 co-ordinates PDGFRα
284 internalisation and its intracellular signalling, as well as the trafficking of integrin α5β1 during cell
285 adhesion (McGowan and McCoy, 2021). Furthermore, it has recently been shown that NRP1 binds to
286 VE-Cadherin and regulates its cell surface turnover, a role that has been proposed to at least partly
287 explain its role in EC barrier integrity (Gioelli et al., 2022, Bosseboeuf et al., 2023). In response to
288 VEGFA the cytoplasmic domain of NRP1, which binds synectin, has been found to be crucial in
289 mediating NRP1's positive regulation of leakage (Fantin et al., 2017). Furthermore, mutant mice
290 lacking the NRP1 cytoplasmic domain have impaired arteriogenesis due to delayed VEGFR2
291 endocytosis and resulting reduction in phosphorylation at Y1175 (Lanahan et al., 2013). Interestingly,

292 the C-terminal tail is also crucial for the stability of trans NRP1-VEGFR2 complexes (Koch et al., 2014).
293 A central function of NRP1 is thus to mediate VEGFR2 internalisation and trafficking following VEGFA
294 stimulation. From our data we hypothesise that NRP1 presented in *trans* delays VEGFR2
295 internalisation and potentiates VEGFR2 signalling upstream of vascular leakage. Indeed, a recent
296 study found that proper internalisation of VEGFR2 is required to shutdown VEGFR2 Y949 signalling
297 through increasing the stoichiometric ratio of cell surface phosphatases that dephosphorylate Y949
298 (Corti et al., 2022). Our data are compatible with the hypothesis that VEGFR2 held at the cell surface
299 via juxtracrine NRP1 interaction is capable of enhancing VEGFR2 Y949 signalling and resulting
300 disruption of EC junctions, but due to the rapid turnover of VEGFR2 phosphorylation, this is
301 technically very challenging to conclusively demonstrate. We hypothesize however that NRP1
302 expression within the perivascular microenvironment could be an important modifying factor of EC
303 signalling and function, and might play an important role in mural cell function during vascular
304 development and quiescence.

305 Combined, we identify a differential function of endothelial NRP1 in VEGFA-mediated
306 vascular leakage in different vascular beds. Different levels and patterning of perivascular NRP1
307 expression has the potential to modify VEGFR2 signalling and alter VEGFA-induced vascular
308 hyperpermeability. Further elucidation of NRP1 expression patterns in different tissues and how the
309 VEGFA/NRP1/VEGFR2 complex presented in *cis* or *trans* can differentially modify cellular signalling
310 will allow to better understand how NRP1 may serve in therapeutic applications in a distinct manner
311 in different tissues.

312

313 **Acknowledgements**

314 We thank the BioVis imaging facility, Uppsala University, for expert services. We appreciate expert
315 advice from Dr. Konstantin Gängel. This study was supported by the Swedish Research Council (2022-
316 00896), the Knut and Alice Wallenberg foundation (KAW 2020.0057 and KAW 2019.0276), Fondation
317 Leducq Transatlantic Network of Excellence Grant in Neurovascular Disease (17 CVD 03) to LCW. MR
318 was supported by Olle Engkvist (218-0057) SSMF (201912) and an EMBO long-term fellowship (ALTF
319 923–2016).

320

321

322

323 **Author contributions**

324 Conceptualization, M.R. and L.C.-W.; methodology, M.R. and S.P.; investigation, M.R., S.P., Y.S.;
325 writing, M.R., S.P. and L.C.-W.; funding acquisition; M.R. and L.C.-W.; resources, L.C.-W.

326 **Conflict of interest**

327 M.R. is now an employee for AstraZeneca (Biopharmaceuticals R&D, Cambridge, UK). All of this work
328 was performed at Dept. of Immunology, Genetics and Pathology, Beijer and Science for Life
329 Laboratories, Uppsala University, Uppsala, Sweden. No funding or support was received from
330 AstraZeneca. Other authors declared no conflict of interest.

331 **Figure legends**

332 **Figure 1: NRP1 regulates VEGFA-mediated permeability in an organotypic manner**

333 **(A)** Schematic illustration of experimental design to induce recombination in *Nrp1* iECKO mice.

334 **(B)** Western blot quantification of lung lysates from tamoxifen-treated control and *Nrp1* iECKO mice
335 (n=4).

336 **(C)** Representative images showing leakage of 2000 kDa FITC-dextran (Pseudo-colour) in response to
337 intradermal VEGFA injection in the ear dermis of control and *Nrp1* iECKO mice.

338 **(D)** Leakage sites per vessel length in response to intradermal VEGFA stimulation in the ear skin of
339 control and *Nrp1* iECKO mice. n=6 mice, two or more acquisitions/mouse.

340 **(E)** Lag period between intradermal VEGFA injection and initiation of leakage in the ear skin of
341 control and *Nrp1* iECKO mice. n≥3 mice, two or more acquisitions/mouse, three or more
342 sites/acquisition.

343 **(F)** Quantification of 2000 kDa dextran extravasation over time in the ear skin of control
344 and *Nrp1* iECKO mice following intradermal VEGFA stimulation. Black lines represent lines of best fit
345 for the slope between leakage initiation and leakage termination. n≥3 mice, two or more
346 acquisitions/mouse, three or more sites/acquisition.

347 **(G-H)** Leakage of fixable 2000 kDa FITC dextran in trachea (G) and back skin (H) after systemic
348 administration of VEGFA in control and *Nrp1* iECKO mice. Left, representative images. Right,
349 quantification of tracer leakage area / vessel area (n ≥ 8 mice, 2 or more fields of view/mouse).

350 **(I-J)** Leakage of 70 kDa (I) and 2000 kDa (J) dextran extracted from perfused tissues after systemic
351 administration of VEGFA in kidney, skeletal muscle and heart in control and *Nrp1* iECKO mice (n ≥ 8
352 mice).

353 Error bars; mean ± SEM. Statistical significance: Two-tailed unpaired student's t-test and linear
354 regression with ANCOVA. Scale bar: 100 µm

355

356 **Figure 2: Global loss of NRP1 reduces VEGFA-mediated vascular permeability**

357 **(A)** Schematic illustration of experimental design to induce recombination in *Nrp1* iKO mice.

358 **(B)** Western blot quantification of lung lysates from tamoxifen-treated control and *Nrp1* iKO mice (n
359 ≥ 2 mice).

360 **(C)** Representative images showing leakage of 2000 kDa FITC dextran (Pseudo-colour) in response to
361 intradermal VEGFA injection in the ear dermis of control and *Nrp1* iKO mice.

362 **(D)** Leakage sites per vessel length in response to intradermal VEGFA stimulation in the ear skin of
363 control and *Nrp1* iKO mice. n=3 mice, two or more acquisitions/mouse.

364 **(E-F)** Leakage of fixable 2000 kDa FITC dextran in trachea (E) and back skin (F) after systemic
365 administration of VEGFA in control and *Nrp1* iKO mice. Left, representative images. Right,
366 quantification of tracer leakage area / vessel area (n ≥ 5 mice, 3 or more fields of view/mouse).

367 Error bars; mean ± SEM. Statistical significance: Two-tailed unpaired student's t-test. Scale bar:
368 100µm

369 **Figure 3: Heterogeneous expression of perivascular NRP1**

370 **(A)** Schematic illusatration of mouse strain and representation of NRP1 expression in endothelial, and
371 perivascular cells using *Pdgfrβ*-GFP mice. White dashed line encompasses vascular area, space
372 between white and yellow dashed lines represents perivascular area. Note perivascular, NRP1
373 expressing cells in between yellow and white lines.

374 **(B-D)** Images, left, and quantification, right, showing vascular and perivascular NRP1 expression in
375 arterioles **(A)**, capillaries **(B)** and venules **(C)** of ear skin and back skin and its relative expression.

376 Error bars; mean ± SEM. Statistical significance: Two-tailed unpaired student's t-test. Scale bar: 50µm

377 **Figure 4: NRP1 distribution modifies VEGFA-induced vascular permeability**

378 **(A)** Schematic illustration of breeding scheme to obtain homozygous *Vegfr2* $^{Y949F/Y949F}$; *Nrp1* iECKO
379 mice and experimental design to induce recombination.

380 **(B)** Western blot quantification of lung lysates from tamoxifen treated *Vegfr2* $^{Y949F/Y949F}$ and *Vegfr2*
381 $^{Y949F/Y949F}$; *Nrp1* iECKO mice (n=3 mice).

382 **(C)** Representative images showing leakage in response to intradermal VEGFA injection in the ear
383 dermis of *Vegfr2* $^{Y949F/Y949F}$ and *Vegfr2* $^{Y949F/Y949F}$; *Nrp1* iECKO mice.

384 **(D)** Leakage sites per vessel length in response to intradermal VEGFA stimulation in the ear skin of in
385 control, *Nrp1* iECKO, *Vegfr2* $^{Y949F/Y949F}$ and *Vegfr2* $^{Y949F/Y949F}$; *Nrp1* iECKO mice, normalized to control (n
386 ≥ 6 mice, two or more acquisitions/mouse).

387 **(E-F)** Leakage of 2000 kDa dextran in trachea (E) and back skin (F) of control, *Nrp1* iECKO, *Vegfr2*
388 $^{Y949F/Y949F}$ and *Vegfr2* $^{Y949F/Y949F}$; *Nrp1* iECKO mice after systemic administration of VEGFA. Left,
389 representative images. Right, quantification of tracer leakage area/vessel area (n ≥ 3 mice, 2 or more
390 fields of view/mouse).

391 Error bars; mean ± SEM. Statistical significance: Two tailed unpaired student's t-test and Two-way
392 ANOVA. Scale bar: 100µm

393 **Figure 5: Perivascular NRP1 modifies VEGFA-induced signalling**

394 **(A-B)** Phosphorylation of VE-Cadherin (VEC) Y685 in response to intradermal PBS or VEGFA injections
395 in the ear dermis of control and *Nrp1* iECKO (A) or *Nrp1* iKO (B) mice. Left, representative images.

396 Right, quantification of phosphorylated VEC Y685 area per total VEC area normalized to PBS control
397 in the ear dermis of control and *Nrp1* iECKO or *Nrp1* iKO mice. n≥3 mice, two or more fields of
398 view/mouse.

399 **(C-D)** Phosphorylation of VE-Cadherin Y685 in response to intradermal PBS or VEGFA injections in the
400 back skin of control and *Nrp1* iECKO (C) or *Nrp1* iKO (D) mice. Left, representative images. Right,
401 quantification of phosphorylated VEC Y685 area per total VEC area normalized to PBS control in the
402 back skin of control and *Nrp1* iECKO or *Nrp1* iKO mice. n≥3 mice, two or more fields of view/mouse.

403 Error bars; mean ± SEM. Statistical significance: Two-way ANOVA. Scale bar: 50µm

404 **Figure 6: Schematic model of NRP1's spatial effects on VEGFA-induced vascular permeability**

405 With global loss of NRP1, VEGFA/VEGFR2 signalling regulating vascular leakage is suppressed and
406 thus leakage is reduced (left). In the presence of EC NRP1, a VEGFA/VEGFR2/NRP1 complex is formed
407 in *cis,* which has a rapid and transient effect on VEGFR2 downstream signalling (middle). Loss of EC
408 NRP1 but the presence of perivascular NRP1 leads to formation of a stable VEGFA/VEGFR2/NRP1
409 complex in *trans* and enhanced VEGFR2 signalling and increased vascular permeability.

410 **Supplementary Figure 1. NRP1 expression in the ear dermis and back skin of adult mice**

411 **(A-B)** Whole mount immunostainings showing NRP1 expression in ear dermis (A) and back skin (B) of
412 control, *Nrp1* iECKO and *Nrp1* iKO mice. Scale bar: 50µm

413 **Supplementary Figure 2. Organotypic assessment of VEGFA-induced leakage**

414 **(A,B)** Leakage of 10 kDa **(A)** and 70 kDa **(B)** dextran after systemic administration of only dextran
415 (control) and dextran plus VEGFA in liver, kidney, skeletal muscle and heart of wild-type C57Bl/6 mice
416 (n ≥ 3 mice).

417 **(C-E)** Leakage of 2000 kDa dextran after systemic administration of only dextran (control) and
418 dextran plus VEGFA in ear dermis **(C)**, back skin **(D)** and trachea **(E)** of wild-type C57Bl/6 mice (n ≥ 2
419 mice).

420 Error bars; mean ± SEM. Statistical significance used: Two-tailed unpaired student's t-test

421 **Supplementary Figure 3. Loss of EC NRP1 reduces VEGFA mediated vascular permeability in the**
422 **back skin**

423 Evans blue leakage with intradermal administration of VEGFA in the back skin of *Nrp1* iECKO mice.
424 Left, representative images. Right, quantification of Evans blue extravasation shown as VEGFA
425 induced leakage fold over PBS (n ≥ 3 mice).

426 Error bars; mean ± SEM. Statistical significance used: Two-tailed unpaired student's t-tes

427 **Supplementary figure 4. Global inactivation of NRP1 reduces VEGFA mediated vascular**
428 **permeability**

429 **(A)** VEGFA-induced leakage in the ear skin of C57Bl/6 mice treated intradermally with isotype control
430 or NRP1 blocking antibody. Left, representative images. Right, quantification of leakage sites per 100
431 µm of vessel length (n=3 mice, 3 acquisitions/mouse).

432 **(B)** Leakage of 2000 kDa dextran in trachea of C57Bl/6 mice treated systemically with isotype control
433 or NRP1 blocking antibody. Left, representative images. Right, quantification of tracer area/vessel
434 area (n=3 mice).

435 **(C)** PBS and VEGFA-induced leakage in the back skin of C57Bl/6 mice treated intradermally with
436 isotype control or NRP1 blocking antibody. Left, representative images. Right, quantification of Evans
437 blue leakage (n=3 mice).

438 Error bars; mean ± SEM. Statistical significance used: Two-tailed unpaired student's t-test. Scale bar:
439 100µm

440 **Supplementary figure 5. Perivascular NRP1 modifies PLCγ phosphorylation**

441 **(A-B)** Phosphorylation of PLCγ in response to intradermal PBS or VEGFA injections in the ear dermis
442 of control and *Nrp1* iECKO (A) or *Nrp1* iKO (B) mice. Left, representative images. Right, quantification
443 of phosphorylated PLCγ area per total VEC area normalized to PBS control in the ear dermis of
444 control and *Nrp1* iECKO or *Nrp1* iKO mice. n≥3 mice, two or more fields of view/mouse.

445 **(C-D)** Phosphorylation of PLCγ in response to intradermal PBS or VEGFA injections in the back skin of
446 control and *Nrp1* iECKO (C) or *Nrp1* iKO (D) mice. Left, representative images. Right, quantification of
447 phosphorylated PLCγ area per total VEC area normalized to PBS control in the back skin of control
448 and *Nrp1* iECKO or *Nrp1* iKO mice. n≥3 mice, two or more fields of view/mouse.

449 Error bars; mean ± SEM. Statistical significance: Two-way ANOVA. Scale bar: 50µm

450 **Methods**

451 Animals

452 *In vivo* animal experiments were carried out in accordance with the ethical permit provided by the
453 Committee on the Ethics of Animal Experiments of the University of Uppsala (permit 6789/18).
454 *Nrp1*$^{flox/flox}$ mice contain *loxP* sites flanking exon 2 and were obtained from The Jackson Laboratory
455 (005247). This strain was crossed with Cdh5(PAC)-CreER^{T2} mice (kind gift from Dr. Ralf Adams, Max-
456 Planck Institute Münster) or Tmem163Tg(ACTB-cre)2Mrt mice to generate endothelial-specific *Nrp1*
457 iECKO mice and global *Nrp1* iKO mice respectively. Mice possessing a knock-in mutation in the VEGFR
458 gene, *Kdr*, at the Y949 phosphosite have been described previously (Li et al., 2016). These mice were
459 crossed with *Nrp1* iECKO mice to generate *Vegfr2* $^{Y949F/Y949F}$*; Nrp1* iECKO mice. *Pdgfrb*-GFP reporter
460 mice (Tg(Pdgfrb-EGFP)jn169Gsat/Mmucd, Stock number 031796-UCD) have been described
461 previously (Jung et al., 2018). Mice were maintained in ventilated cages with group housing (2–5 per
462 cage) and access to water and feed ad libitum. Male and female mice age 8-18 weeks were used.
463 Each experiment was conducted on tissue from at least three age-matched animals representing
464 individual biological repeats. Sample size (number of acquired images / movies and number of mice)
465 were chosen to ensure reproducibility and allow stringent statistical analysis. To induce Cre
466 recombinase-mediated gene recombination tamoxifen (SigmaAldrich, T5648) formulated in peanut
467 oil was injected intraperitoneally (80 mg/kg) for 5 consecutive days. The mice were allowed to rest
468 for 4 days before experiments were conducted.

469

470 Intravital vascular leakage assay

471 Intravital imaging of the mouse ear with intradermal injection has been described previously
472 (Honkura et al., 2018). Briefly, following systemic administration of 2000 kDa FITC (SigmaAldrich,
473 FD2000S) or TRITC Dextran (ThermoFischer Scientific, D7139) by tail-vein injection, mice were
474 sedated by intraperitoneal injection of Ketamine-Xylazine (120 mg/kg Ketamine, 10 mg/kg Xylazine)
475 and the ear secured to a solid support. Mice were maintained at a body temperature of 37 °C for the
476 entire experiment, maximum 90 min. Time-lapse imaging was performed using single-photon
477 microscopy (Leica SP8). For intradermal EC stimulation, a volume of approximately 0.1 µl VEGFA
478 (Peprotech, 450-32), concentration 100 ng/µl, was injected using a sub-micrometer capillary needle.
479 10 kDa TRITC Dextran (ThermoFischer Scientific, D1817) was used as a tracer. Leakage sites were
480 identified in time-lapse imaging as defined sites of concentrated dextran in the extravascular space.
481

482 Miles' assay

483 Mice were injected intraperitoneally with pyrilamine maleate salt (4mg/kg, Sigma, P5514) diluted in
484 0.9% saline, to inhibit histamine release, 30 min prior to tail vein injection of Evans blue (100 µl, 1%
485 Evans blue). Evans blue was allowed to circulate for 10 min before intradermal injection in the back
486 skin of recombinant mouse VEGFA165 (Peprotech, 450-32) (80 ng in 25 µl) or PBS. The skin was
487 excised 30 minutes subsequent to VEGFA injection, placed in formamide over night at 55°C and
488 absorbance at 620nm was measured using a spectrophotometer and normalized to tissue weight.
489

490 Systemic VEGFA-induced permeability

491 To assess EC permeability, all tissues were cleaned of excess cartilage, fat and connective tissue.
492 Skeletal muscle was assessed using the tibialis anterior and liver was assessed using the left lateral
493 lobe. To analyse liver, kidney, skeletal muscle and heart permeability, dextran (30 mg/kg) with or
494 without VEGFA (160 µg/kg) were injected systemically through the tail vein. Thirty minutes later mice
495 were anesthetized with Ketamine/Xylazine before intracardiac perfusion with Dulbecco's phosphate
496 buffered saline (DPBS). Tissues were dissected, washed in DPBS and incubated in formamide for 48
497 hr at 55 °C. Dextran fluorescence was then measured using a spectrophotometer and normalized to
498 tissue weight. To assess VEGFA-induced leakage microscopically, mixtures of fixable dextran (FITC,
499 Tdb labs; TRITC, ThermoFischer Scientific, D7139) (30 mg/kg) with VEGFA (160 µg/kg) were injected
500 systemically through the tail vein. Thirty minutes later mice were anesthetized with
501 Ketamine/Xylazine before intracardiac perfusion with DPBS followed by 1% paraformaldehyde.
502 Tissues were then immersed in 1% paraformaldehyde for 2 hr before proceeding with
503 immunohistochemistry. For leakage quantification at least three large tile scan areas (≥1 mm^2) were
504 captured for each mouse.

505

506 Intradermal VEGFA injection in the ear and back skin

507 Mice were anesthetised using isofluorane and injected with PBS or VEGFA (Peprotech, 450-32) (20ug
508 in 5 ul for the ear dermis and 80ug in 20ul for the back skin) followed by perfusion using 1% PFA. The
509 ear and back skin samples were excised and further fixed for 1 hour in 1% PFA. Afterwards, the tissue
510 samples were processed for immunostaining.

511

512 NRP1 blockade

513 Anti-NRP1 (R&D systems, MAB59941) or isotype control (R&D Systems, MAB006) were administered
514 intradermally in the ear skin (1 µg) or back skin (5 µg), or systemically (2 mg/kg). 24 hours later
515 VEGFA-mediated vascular leakage was assessed using the intravital vascular leakage assay, Miles'
516 assay or through systemic VEGFA-induced permeability.

517

518 Immunohistochemistry

519 Tissues were fixed through intracardiac perfusion with 1% paraformaldehyde (PFA) followed by
520 immersion in 1% PFA for 2 hr at room temperature. For whole mount preparation of the ear skin,
521 back skin and trachea removal of excess cartilage, fat and connective tissue tissues was carried out.
522 Tissues were blocked overnight at 4 °C in Tris-buffered saline (TBS), 5% (w/v) Bovine Serum Albumin
523 (BSA), 0.2% Triton X-100. Samples were incubated overnight with primary antibody in blocking
524 solution, followed by washing in TBS, 0.2% Triton X-100 and incubation with appropriate secondary
525 antibody for 2 hr at room temperature in blocking buffer before washing and mounting in
526 fluorescent mounting medium (DAKO). Images were acquired using a Leica SP8 confocal microscope.
527 Commercial antibodies used were: rat anti-CD31 (BD Biosciences, 553370), goat anti-CD31 (R&D
528 Systems, AF3628), goat anti-NRP1 (R&D Systems, AF566), chicken anti-GFP (Abcam, Ab13970), rabbit
529 anti-phospho-PLCγ1 (Tyr783) (Cell signaling technology, 2821s), rabbit anti-PLCγ1 (Cell signaling
530 technology, 2822s), and goat anti–VE-cadherin (R&D systems, AF1002). Secondary antibodies against
531 rat (ThermoFischer Scientific; Alexa 488, A21208 and Alexa 594, A21209), rabbit (ThermoFischer
532 Scientific; Alexa 488, A21206 and Alexa 568, A10042), goat (ImmunoResearch Laboratories, Alexa
533 647, 705-605-147), chicken (ImmunoResearch Laboratories, Alexa 488, 703-545-155) were used.
534 pVEC Y685 antibody was prepared by immunizing rabbits with phospho-peptides of the
535 corresponding region in mouse VE-cadherin (New England Peptide) and further verified using
536 immunostaining in Cdh5$^{Y685F/Y685F}$ mice. Primary and secondary antibodies were prepared at a dilution
537 of 1:100 and 1:400, respectively unless otherwise stated.

538

539 Western blot analysis

540 Lungs from mice were removed and snap frozen. Protein was obtained by mechanical dissociation in
541 RIPA buffer supplemented with 50 nM Na3VO4, Phosphatase inhibitor cocktail (Roche 04906837001)
542 and Protease inhibitor cocktail (Roche, 04693116001). LDS sample buffer (Invitrogen, NP0007) and
543 Sample Reducing Agent (Invitrogen, NP0009) were added to the samples and heated to 70 °C for 10
544 min. Proteins were separated on Nu Page 4–12% Bis-Tris Gel (Invitrogen) in MOPS SDS Running
545 buffer (Invitrogen, NP0001), transferred to PVDF membrane (Thermo scientific, 88518) in NuPAGE
546 transfer buffer (Novex, NP006), 10% methanol and subsequently blocked with 5% BSA in Tris-
547 buffered saline with Tween 20 (TBST) for 60 min. The immunoblots were analysed using primary
548 antibodies incubated overnight at 4 °C and secondary antibodies linked to horseradish peroxidase
549 (HRP) (Cytiva) incubated for 1 hr at room temperature. After each step filters were washed four
550 times with TBST. HRP signals were visualized by enhanced chemiluminescence (ECL) (Cytiva)
551 (1:25000) and imaged with Chemidoc (Bio-Rad).
552 Primary antibodies targeting GAPDH (Chemicon, MONOCLONAL ANTIBODY374), NRP1 (R&D Systems,
553 AF566) were used at a dilution of 1:1,000.

554

555 Image quantification

556 For confocal images, macromolecular leakage was quantified by measurement of tracer area
557 following image thresholding. Tracer area was then normalized to vessel area. For analysis of
558 vascular and peri-vascular NRP1 expression, masks were generated of the CD31 vascular area and the
559 peri-vascular area 3µm around the vessel (Figure 3A). NRP1 area following thresholding was
560 quantified within, and normalised to these areas. Phosphorylation values were quantified by
561 measurement of phosphorylated vessel area following image thresholding. Phosphorylation area was
562 then normalized to vessel area. Threshold values were kept constant within experiments.
563 Analysis of leakage from intravital movies has been described previously (Richards et al., 2021).
564 Briefly, leakage sites were identified in time-lapse imaging as defined sites of concentrated dextran in
565 the extravascular space. To quantify these their numbers were normalized to vessel length. To assess
566 lag period the time of the appearance of these sites following injection of stimulus was quantified. To
567 assess the extent of barrier disruption the rate of dextran extravasation specifically at these sites was
568 quantified over time.
569 All measurements were done with Fiji processing package of Image J2 software.

570

571 Statistical analysis

572 Data are expressed as mean ± SEM. The statistical tests used were the Students't test and two-way
573 ANOVA. P-values given are from independent samples analysed by two-tailed paired t tests or
574 multiple comparisons obtained from two-way ANOVA. Rate of leakage was compared using linear
575 regression and ANCOVA. All statistical analyses were conducted using GraphPad Prism. A p-value
576 <0.05 was considered statistically significant and significances indicated as p<0.05 (*), p<0.01 (**),
577 and p<0.001 (***). For animal experiments, no statistical methods were used to predetermine
578 sample size. The investigators were blinded to allocation during experiment and outcome
579 assessment.

580

581 **References**

582 ACEVEDO, L. M., BARILLAS, S., WEIS, S. M., GÖTHERT, J. R. & CHERESH, D. A. 2008. Semaphorin 3A
583 suppresses VEGF-mediated angiogenesis yet acts as a vascular permeability factor. *Blood,*
584 111**,** 2674-80.
585 AIRD, W. C. 2007. Phenotypic heterogeneity of the endothelium: I. Structure, function, and
586 mechanisms. *Circ Res,* 100**,** 158-73.
587 AUGUSTIN, H. G. & KOH, G. Y. 2017. Organotypic vasculature: From descriptive heterogeneity to
588 functional pathophysiology. *Science,* 357.
589 BALLMER-HOFER, K., ANDERSSON, A. E., RATCLIFFE, L. E. & BERGER, P. 2011. Neuropilin-1 promotes
590 VEGFR-2 trafficking through Rab11 vesicles thereby specifying signal output. *Blood,* 118**,** 816-
591 26.
592 BARTLETT, C. S., SCOTT, R. P., CAROTA, I. A., WNUK, M. L., KANWAR, Y. S., MINER, J. H. & QUAGGIN,
593 S. E. 2017. Glomerular mesangial cell recruitment and function require the co-receptor
594 neuropilin-1. *Am J Physiol Renal Physiol,* 313**,** F1232-F1242.
595 BAYLISS, A. L., SUNDARARAMAN, A., GRANET, C. & MELLOR, H. 2020. Raftlin is recruited by
596 neuropilin-1 to the activated VEGFR2 complex to control proangiogenic signaling.
597 *Angiogenesis,* 23**,** 371-383.
598 BECKER, P. M., WALTENBERGER, J., YACHECHKO, R., MIRZAPOIAZOVA, T., SHAM, J. S., LEE, C. G.,
599 ELIAS, J. A. & VERIN, A. D. 2005. Neuropilin-1 regulates vascular endothelial growth factor-
600 mediated endothelial permeability. *Circ Res,* 96**,** 1257-65.
601 BOSSEBOEUF, E., CHIKH, A., CHAKER, A. B., MITCHELL, T. P., VIGNARAJA, D., RAJENDRAKUMAR, R.,
602 KHAMBATA, R. S., NIGHTINGALE, T. D., MASON, J. C., RANDI, A. M., AHLUWALIA, A. &
603 RAIMONDI, C. 2023. Neuropilin-1 interacts with VE-cadherin and TGFBR2 to stabilize
604 adherens junctions and prevent activation of endothelium under flow. *Sci Signal,* 16**,**
605 eabo4863.
606 CAI, H. & REED, R. R. 1999. Cloning and characterization of neuropilin-1-interacting protein: a PSD-
607 95/Dlg/ZO-1 domain-containing protein that interacts with the cytoplasmic domain of
608 neuropilin-1. *J Neurosci,* 19**,** 6519-27.
609 CERANI, A., TETREAULT, N., MENARD, C., LAPALME, E., PATEL, C., SITARAS, N., BEAUDOIN, F.,
610 LEBOEUF, D., DE GUIRE, V., BINET, F., DEJDA, A., REZENDE, F. A., MILOUDI, K. & SAPIEHA, P.
611 2013. Neuron-derived semaphorin 3A is an early inducer of vascular permeability in diabetic
612 retinopathy via neuropilin-1. *Cell Metab,* 18**,** 505-18.
613 CORTI, F., RISTORI, E., RIVERA-MOLINA, F., TOOMRE, D., ZHANG, J., MIHAILOVIC, J., ZHUANG, Z. W. &
614 SIMONS, M. 2022. Syndecan-2 selectively regulates VEGF-induced vascular permeability.
615 *Nature Cardiovascular Research,* 1**,** 518-528.

616 FANTIN, A., LAMPROPOULOU, A., SENATORE, V., BRASH, J. T., PRAHST, C., LANGE, C. A., LIYANAGE, S.
617 E., RAIMONDI, C., BAINBRIDGE, J. W., AUGUSTIN, H. G. & RUHRBERG, C. 2017. VEGF165-
618 induced vascular permeability requires NRP1 for ABL-mediated SRC family kinase activation. *J*
619 *Exp Med,* 214**,** 1049-1064.
620 FERNÁNDEZ-ROBREDO, P., SELVAM, S., POWNER, M. B., SIM, D. A. & FRUTTIGER, M. 2017. Neuropilin
621 1 Involvement in Choroidal and Retinal Neovascularisation. *PLoS One,* 12**,** e0169865.
622 GIOELLI, N., NEILSON, L. J., WEI, N., VILLARI, G., CHEN, W., KUHLE, B., EHLING, M., MAIONE, F.,
623 WILLOX, S., BRUNDU, S., AVANZATO, D., KOULOURAS, G., MAZZONE, M., GIRAUDO, E., YANG,
624 X. L., VALDEMBRI, D., ZANIVAN, S. & SERINI, G. 2022. Neuropilin 1 and its inhibitory ligand
625 mini-tryptophanyl-tRNA synthetase inversely regulate VE-cadherin turnover and vascular
626 permeability. *Nat Commun,* 13**,** 4188.
627 GOSHIMA, Y., HORI, H., SASAKI, Y., YANG, T., KAGOSHIMA-MAEZONO, M., LI, C., TAKENAKA, T.,
628 NAKAMURA, F., TAKAHASHI, T., STRITTMATTER, S. M., MISU, Y. & KAWAKAMI, T. 1999.
629 Growth cone neuropilin-1 mediates collapsin-1/Sema III facilitation of antero- and retrograde
630 axoplasmic transport. *J Neurobiol,* 39**,** 579-89.
631 GU, C., LIMBERG, B. J., WHITAKER, G. B., PERMAN, B., LEAHY, D. J., ROSENBAUM, J. S., GINTY, D. D. &
632 KOLODKIN, A. L. 2002. Characterization of neuropilin-1 structural features that confer
633 binding to semaphorin 3A and vascular endothelial growth factor 165. *J Biol Chem,* 277**,**
634 18069-76.
635 HONG, T. M., CHEN, Y. L., WU, Y. Y., YUAN, A., CHAO, Y. C., CHUNG, Y. C., WU, M. H., YANG, S. C.,
636 PAN, S. H., SHIH, J. Y., CHAN, W. K. & YANG, P. C. 2007. Targeting neuropilin 1 as an
637 antitumor strategy in lung cancer. *Clin Cancer Res,* 13**,** 4759-68.
638 HONKURA, N., RICHARDS, M., LAVINA, B., SAINZ-JASPEADO, M., BETSHOLTZ, C. & CLAESSON-WELSH,
639 L. 2018. Intravital imaging-based analysis tools for vessel identification and assessment of
640 concurrent dynamic vascular events. *Nat Commun,* 9**,** 2746.
641 HOROWITZ, A. & SEERAPU, H. R. 2012. Regulation of VEGF signaling by membrane traffic. *Cell Signal,*
642 24**,** 1810-20.
643 HU, B., GUO, P., BAR-JOSEPH, I., IMANISHI, Y., JARZYNKA, M. J., BOGLER, O., MIKKELSEN, T., HIROSE,
644 T., NISHIKAWA, R. & CHENG, S. Y. 2007. Neuropilin-1 promotes human glioma progression
645 through potentiating the activity of the HGF/SF autocrine pathway. *Oncogene,* 26**,** 5577-86.
646 JIN, Y., DING, Y., RICHARDS, M., KAAKINEN, M., GIESE, W., BAUMANN, E., SZYMBORSKA, A., ROSA, A.,
647 NORDLING, S., SCHIMMEL, L., AKMERIÇ, E. B., PENA, A., NWADOZI, E., JAMALPOUR, M.,
648 HOLSTEIN, K., SÁINZ-JASPEADO, M., BERNABEU, M. O., WELSH, M., GORDON, E., FRANCO, C.
649 A., VESTWEBER, D., EKLUND, L., GERHARDT, H. & CLAESSON-WELSH, L. 2022. Tyrosine-
650 protein kinase Yes controls endothelial junctional plasticity and barrier integrity by regulating
651 VE-cadherin phosphorylation and endocytosis. *Nature Cardiovascular Research,* 1**,** 1156-
652 1173.
653 JUNG, B., ARNOLD, T. D., RASCHPERGER, E., GAENGEL, K. & BETSHOLTZ, C. 2018. Visualization of
654 vascular mural cells in developing brain using genetically labeled transgenic reporter mice. *J*
655 *Cereb Blood Flow Metab,* 38**,** 456-468.
656 KAWAKAMI, T., TOKUNAGA, T., HATANAKA, H., KIJIMA, H., YAMAZAKI, H., ABE, Y., OSAMURA, Y.,
657 INOUE, H., UEYAMA, Y. & NAKAMURA, M. 2002. Neuropilin 1 and neuropilin 2 co-expression
658 is significantly correlated with increased vascularity and poor prognosis in nonsmall cell lung
659 carcinoma. *Cancer,* 95**,** 2196-201.
660 KAWASAKI, T., KITSUKAWA, T., BEKKU, Y., MATSUDA, Y., SANBO, M., YAGI, T. & FUJISAWA, H. 1999. A
661 requirement for neuropilin-1 in embryonic vessel formation. *Development,* 126**,** 4895-902.
662 KITSUKAWA, T., SHIMONO, A., KAWAKAMI, A., KONDOH, H. & FUJISAWA, H. 1995. Overexpression of
663 a membrane protein, neuropilin, in chimeric mice causes anomalies in the cardiovascular
664 system, nervous system and limbs. *Development,* 121**,** 4309-18.
665 KOCH, S., VAN MEETEREN, L. A., MORIN, E., TESTINI, C., WESTRÖM, S., BJÖRKELUND, H., LE JAN, S.,
666 ADLER, J., BERGER, P. & CLAESSON-WELSH, L. 2014. NRP1 presented in trans to the

667 endothelium arrests VEGFR2 endocytosis, preventing angiogenic signaling and tumor
668 initiation. *Dev Cell,* 28**,** 633-46.
669 LANAHAN, A., ZHANG, X., FANTIN, A., ZHUANG, Z., RIVERA-MOLINA, F., SPEICHINGER, K., PRAHST, C.,
670 ZHANG, J., WANG, Y., DAVIS, G., TOOMRE, D., RUHRBERG, C. & SIMONS, M. 2013. The
671 neuropilin 1 cytoplasmic domain is required for VEGF-A-dependent arteriogenesis. *Dev Cell,*
672 25**,** 156-68.
673 LANAHAN, A. A., HERMANS, K., CLAES, F., KERLEY-HAMILTON, J. S., ZHUANG, Z. W., GIORDANO, F. J.,
674 CARMELIET, P. & SIMONS, M. 2010. VEGF receptor 2 endocytic trafficking regulates arterial
675 morphogenesis. *Dev Cell,* 18**,** 713-24.
676 LI, X., PADHAN, N., SJÖSTRÖM, E. O., ROCHE, F. P., TESTINI, C., HONKURA, N., SÁINZ-JASPEADO, M.,
677 GORDON, E., BENTLEY, K., PHILIPPIDES, A., TOLMACHEV, V., DEJANA, E., STAN, R. V.,
678 VESTWEBER, D., BALLMER-HOFER, K., BETSHOLTZ, C., PIETRAS, K., JANSSON, L. & CLAESSON-
679 WELSH, L. 2016. VEGFR2 pY949 signalling regulates adherens junction integrity and
680 metastatic spread. *Nat Commun,* 7**,** 11017.
681 MAMLUK, R., GECHTMAN, Z., KUTCHER, M. E., GASIUNAS, N., GALLAGHER, J. & KLAGSBRUN, M.
682 2002. Neuropilin-1 binds vascular endothelial growth factor 165, placenta growth factor-2,
683 and heparin via its b1b2 domain. *J Biol Chem,* 277**,** 24818-25.
684 MATSUMOTO, T., BOHMAN, S., DIXELIUS, J., BERGE, T., DIMBERG, A., MAGNUSSON, P., WANG, L.,
685 WIKNER, C., QI, J. H., WERNSTEDT, C., WU, J., BRUHEIM, S., MUGISHIMA, H.,
686 MUKHOPADHYAY, D., SPURKLAND, A. & CLAESSON-WELSH, L. 2005. VEGF receptor-2 Y951
687 signaling and a role for the adapter molecule TSAd in tumor angiogenesis. *Embo j,* 24**,** 2342-
688 53.
689 MCGOWAN, S. E. & MCCOY, D. M. 2021. Neuropilin-1 directs PDGFRalpha-entry into lung fibroblasts
690 and signaling from very early endosomes. *Am J Physiol Lung Cell Mol Physiol,* 320**,** L179-L192.
691 MIAO, H. Q., LEE, P., LIN, H., SOKER, S. & KLAGSBRUN, M. 2000. Neuropilin-1 expression by tumor
692 cells promotes tumor angiogenesis and progression. *FASEB J,* 14**,** 2532-9.
693 MORIN, E., LINDSKOG, C., JOHANSSON, M., EGEVAD, L., SANDSTRÖM, P., HARMENBERG, U.,
694 CLAESSON-WELSH, L. & SJÖBERG, E. 2020. Perivascular Neuropilin-1 expression is an
695 independent marker of improved survival in renal cell carcinoma. *The Journal of Pathology,*
696 250**,** 387-396.
697 MORIN, E., SJÖBERG, E., TJOMSLAND, V., TESTINI, C., LINDSKOG, C., FRANKLIN, O., SUND, M.,
698 ÖHLUND, D., KIFLEMARIAM, S., SJÖBLOM, T. & CLAESSON-WELSH, L. 2018. VEGF receptor-
699 2/neuropilin 1 trans-complex formation between endothelial and tumor cells is an
700 independent predictor of pancreatic cancer survival. *The Journal of Pathology,* 246**,** 311-322.
701 NACCACHE, S. N., HASSON, T. & HOROWITZ, A. 2006. Binding of internalized receptors to the PDZ
702 domain of GIPC/synectin recruits myosin VI to endocytic vesicles. *Proc Natl Acad Sci U S A,*
703 103**,** 12735-40.
704 ORSENIGO, F., GIAMPIETRO, C., FERRARI, A., CORADA, M., GALAUP, A., SIGISMUND, S., RISTAGNO,
705 G., MADDALUNO, L., KOH, G. Y., FRANCO, D., KURTCUOGLU, V., POULIKAKOS, D., BALUK, P.,
706 MCDONALD, D., GRAZIA LAMPUGNANI, M. & DEJANA, E. 2012. Phosphorylation of VE-
707 cadherin is modulated by haemodynamic forces and contributes to the regulation of vascular
708 permeability in vivo. *Nat Commun,* 3**,** 1208.
709 PAN, Q., CHANTHERY, Y., LIANG, W. C., STAWICKI, S., MAK, J., RATHORE, N., TONG, R. K., KOWALSKI,
710 J., YEE, S. F., PACHECO, G., ROSS, S., CHENG, Z., LE COUTER, J., PLOWMAN, G., PEALE, F.,
711 KOCH, A. W., WU, Y., BAGRI, A., TESSIER-LAVIGNE, M. & WATTS, R. J. 2007. Blocking
712 neuropilin-1 function has an additive effect with anti-VEGF to inhibit tumor growth. *Cancer*
713 *Cell,* 11**,** 53-67.
714 PONUWEI, G. A. 2016. A glimpse of the ERM proteins. *J Biomed Sci,* 23**,** 35.
715 RAIMONDI, C., FANTIN, A., LAMPROPOULOU, A., DENTI, L., CHIKH, A. & RUHRBERG, C. 2014. Imatinib
716 inhibits VEGF-independent angiogenesis by targeting neuropilin 1-dependent ABL1 activation
717 in endothelial cells. *J Exp Med,* 211**,** 1167-83.

718 RICHARDS, M., NWADOZI, E., PAL, S., MARTINSSON, P., KAAKINEN, M., GLOGER, M., SJÖBERG, E.,
719 KOLTOWSKA, K., BETSHOLTZ, C., EKLUND, L., NORDLING, S. & CLAESSON-WELSH, L. 2022.
720 Claudin5 protects the peripheral endothelial barrier in an organ and vessel-type-specific
721 manner. *Elife,* 11.
722 RICHARDS, M., PAL, S., SJÖBERG, E., MARTINSSON, P., VENKATRAMAN, L. & CLAESSON-WELSH, L.
723 2021. Intra-vessel heterogeneity establishes enhanced sites of macromolecular leakage
724 downstream of laminin α5. *Cell Rep,* 35**,** 109268.
725 ROTH, L., PRAHST, C., RUCKDESCHEL, T., SAVANT, S., WESTRÖM, S., FANTIN, A., RIEDEL, M.,
726 HÉROULT, M., RUHRBERG, C. & AUGUSTIN, H. G. 2016. Neuropilin-1 mediates vascular
727 permeability independently of vascular endothelial growth factor receptor-2 activation. *Sci*
728 *Signal,* 9**,** ra42.
729 SARRIS, M., ANDERSEN, K. G., RANDOW, F., MAYR, L. & BETZ, A. G. 2008. Neuropilin-1 expression on
730 regulatory T cells enhances their interactions with dendritic cells during antigen recognition.
731 *Immunity,* 28**,** 402-13.
732 SHAHRABI-FARAHANI, S., GALLOTTINI, M., MARTINS, F., LI, E., MUDGE, D. R., NAKAYAMA, H., HIDA,
733 K., PANIGRAHY, D., D'AMORE, P. A. & BIELENBERG, D. R. 2016. Neuropilin 1 Receptor Is Up-
734 Regulated in Dysplastic Epithelium and Oral Squamous Cell Carcinoma. *Am J Pathol,* 186**,**
735 1055-64.
736 SHERAFAT, A., PFEIFFER, F., REISS, A. M., WOOD, W. M. & NISHIYAMA, A. 2021. Microglial neuropilin-
737 1 promotes oligodendrocyte expansion during development and remyelination by trans-
738 activating platelet-derived growth factor receptor. *Nat Commun,* 12**,** 2265.
739 SJOBERG, E., MELSSEN, M., RICHARDS, M., DING, Y., CHANOCA, C., CHEN, D., NWADOZI, E., PAL, S.,
740 LOVE, D. T., NINCHOJI, T., SHIBUYA, M., SIMONS, M., DIMBERG, A. & CLAESSON-WELSH, L.
741 2023. Endothelial VEGFR2-PLCgamma signaling regulates vascular permeability and
742 antitumor immunity through eNOS/Src. *J Clin Invest,* 133.
743 SOKER, S., MIAO, H. Q., NOMI, M., TAKASHIMA, S. & KLAGSBRUN, M. 2002. VEGF165 mediates
744 formation of complexes containing VEGFR-2 and neuropilin-1 that enhance VEGF165-
745 receptor binding. *J Cell Biochem,* 85**,** 357-68.
746 SUN, Z., LI, X., MASSENA, S., KUTSCHERA, S., PADHAN, N., GUALANDI, L., SUNDVOLD-GJERSTAD, V.,
747 GUSTAFSSON, K., CHOY, W. W., ZANG, G., QUACH, M., JANSSON, L., PHILLIPSON, M., ABID,
748 M. R., SPURKLAND, A. & CLAESSON-WELSH, L. 2012. VEGFR2 induces c-Src signaling and
749 vascular permeability in vivo via the adaptor protein TSAd. *J Exp Med,* 209**,** 1363-77.
750 WANG, J., WANG, S., LI, M., WU, D., LIU, F., YANG, R., JI, S., JI, A. & LI, Y. 2015. The Neuropilin-1
751 Inhibitor, ATWLPPR Peptide, Prevents Experimental Diabetes-Induced Retinal Injury by
752 Preserving Vascular Integrity and Decreasing Oxidative Stress. *PLoS One,* 10**,** e0142571.
753 WESSEL, F., WINDERLICH, M., HOLM, M., FRYE, M., RIVERA-GALDOS, R., VOCKEL, M., LINNEPE, R., IPE,
754 U., STADTMANN, A., ZARBOCK, A., NOTTEBAUM, A. F. & VESTWEBER, D. 2014. Leukocyte
755 extravasation and vascular permeability are each controlled in vivo by different tyrosine
756 residues of VE-cadherin. *Nat Immunol,* 15**,** 223-30.
757 WNUK, M., ANDEREGG, M. A., GRABER, W. A., BUERGY, R., FUSTER, D. G. & DJONOV, V. 2017.
758 Neuropilin1 regulates glomerular function and basement membrane composition through
759 pericytes in the mouse kidney. *Kidney Int,* 91**,** 868-879.

760

Figure 1

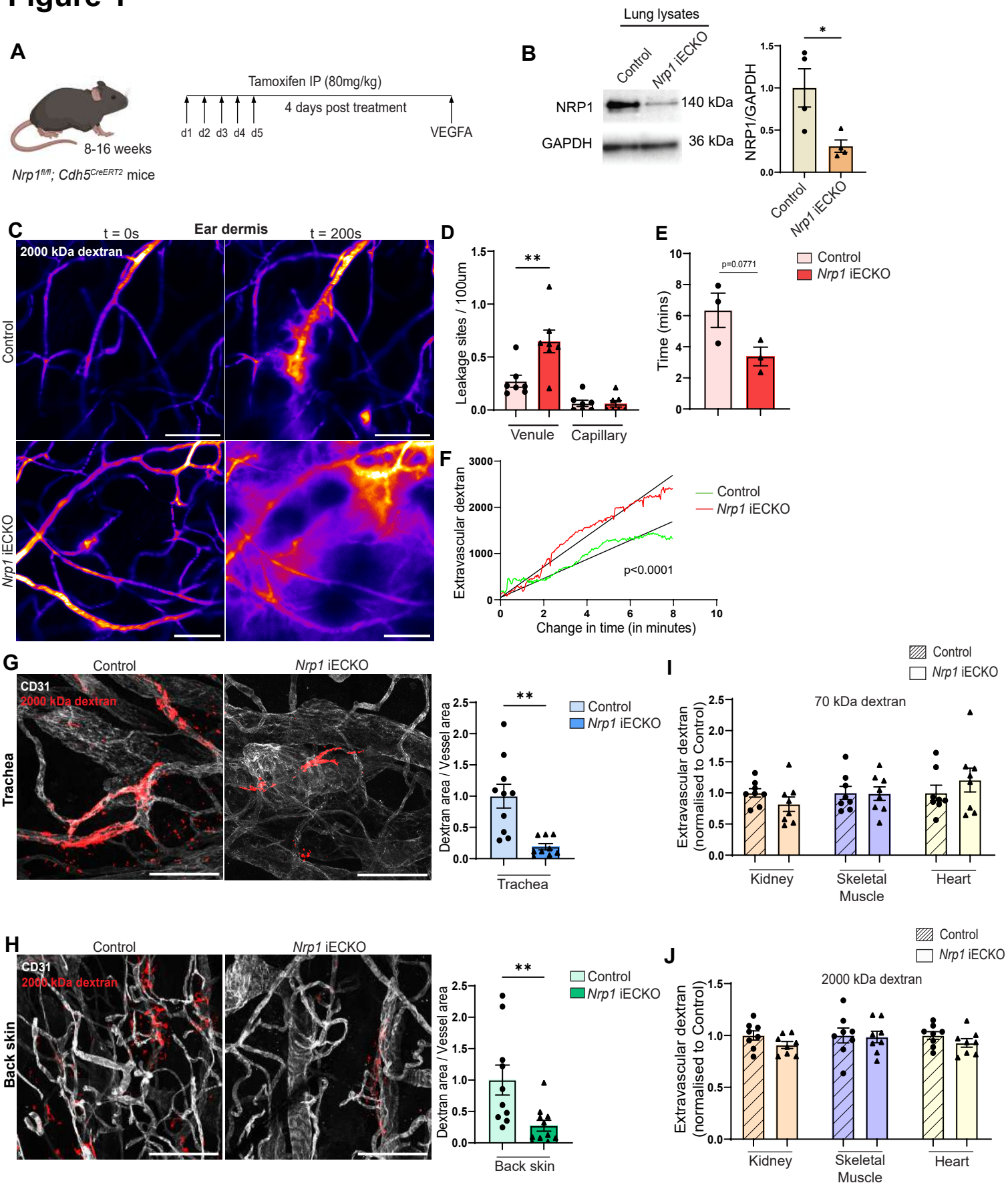
A
8-16 weeks
Nrp1fl/fl; Cdh5CreERT2 mice
Tamoxifen IP (80mg/kg)
4 days post treatment
d1 d2 d3 d4 d5
VEGFA
B
Lung lysates
Control
Nrp1 iECKO
NRP1
GAPDH
140 kDa
36 kDa
NRP1/GAPDH
*
C
t = 0s
Ear dermis
t = 200s
2000 kDa dextran
Control
Nrp1 iECKO
D
Leakage sites / 100um
**
Venule
Capillary
E
Time (mins)
p=0.0771
Control
Nrp1 iECKO
F
Extravascular dextran
Control
Nrp1 iECKO
p<0.0001
Change in time (in minutes)
G
Control
Nrp1 iECKO
CD31
2000 kDa dextran
Trachea
Dextran area / Vessel area
**
Trachea
I
70 kDa dextran
Extravascular dextran (normalised to Control)
Kidney
Skeletal Muscle
Heart
H
Control
Nrp1 iECKO
CD31
2000 kDa dextran
Back skin
Dextran area / Vessel area
**
Back skin
J
2000 kDa dextran
Extravascular dextran (normalised to Control)
Kidney
Skeletal Muscle
Heart

Figure 2

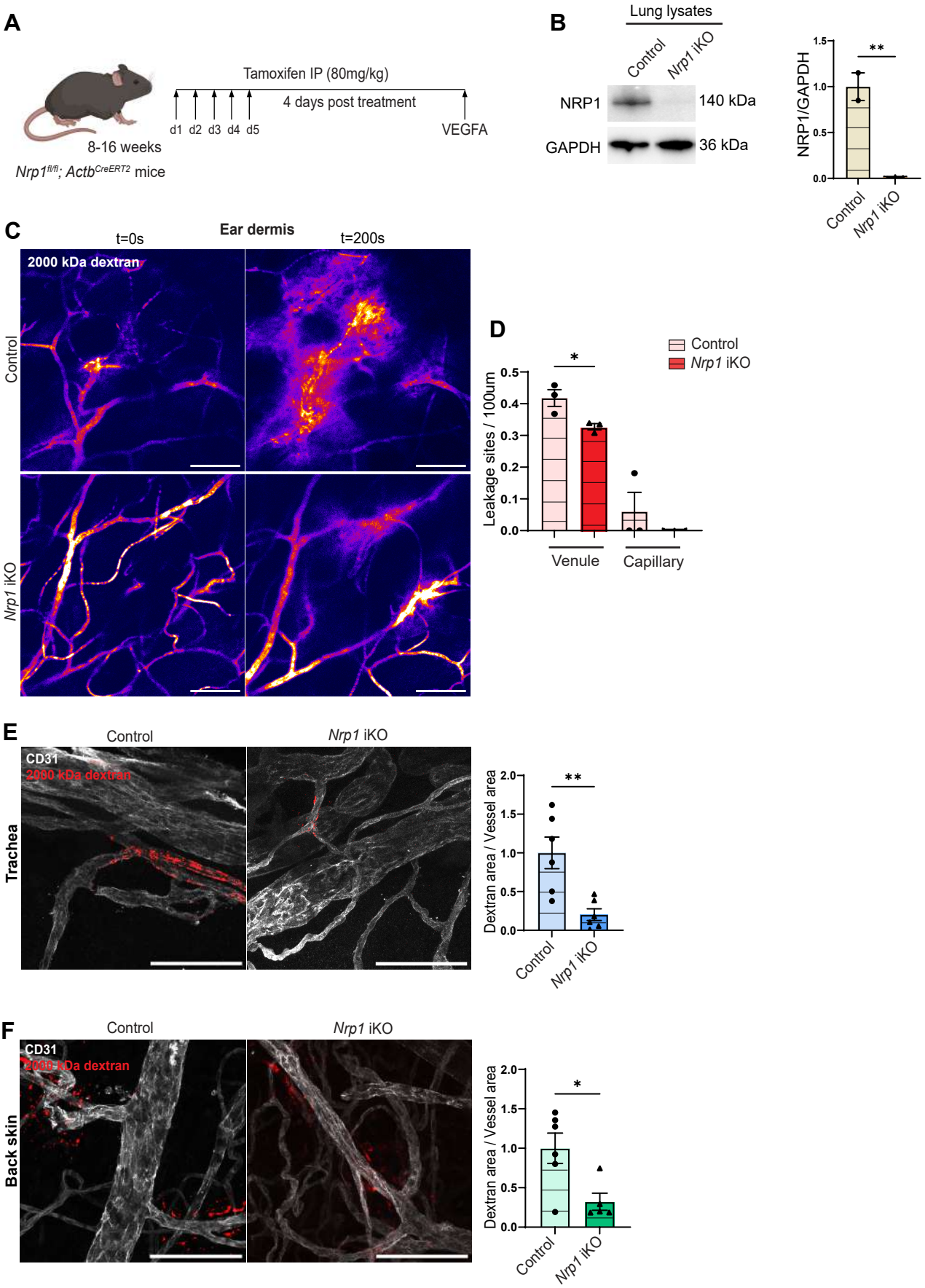
A
Tamoxifen IP (80mg/kg)
4 days post treatment
d1 d2 d3 d4 d5
VEGFA
8-16 weeks
Nrp1fl/fl; ActbCreERT2 mice
B
Lung lysates
Control
Nrp1 iKO
NRP1
140 kDa
GAPDH
36 kDa
NRP1/GAPDH
**
C
t=0s
Ear dermis
t=200s
2000 kDa dextran
Control
Nrp1 iKO
D
Control
Nrp1 iKO
Leakage sites / 100um
*
Venule
Capillary
E
Control
Nrp1 iKO
CD31
2000 kDa dextran
Trachea
Dextran area / Vessel area
**
F
Control
Nrp1 iKO
CD31
2000 kDa dextran
Back skin
Dextran area / Vessel area
*

Figure 3

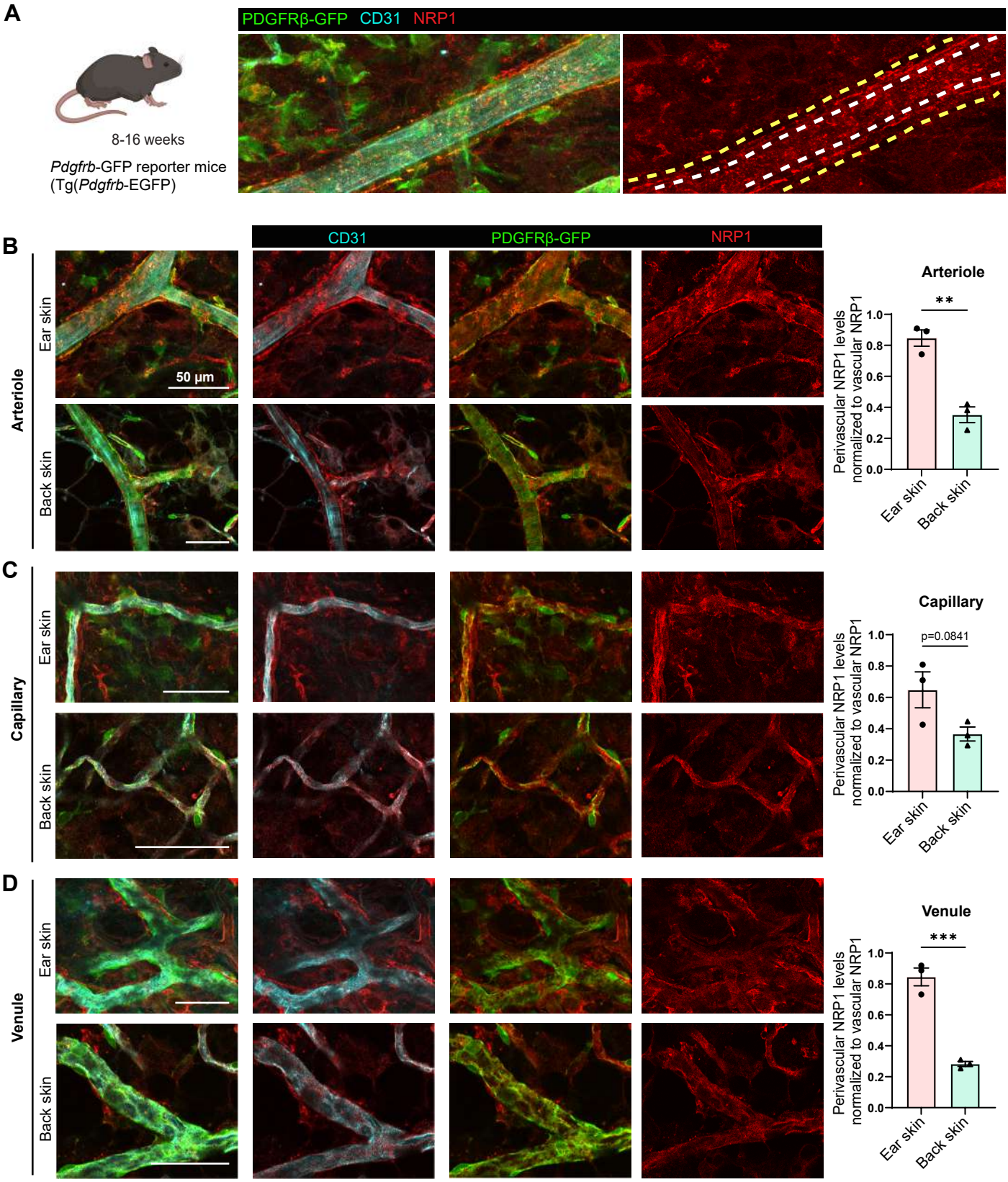
A
PDGFRβ-GFP CD31 NRP1
8-16 weeks
Pdgfrb-GFP reporter mice
(Tg(*Pdgfrb*-EGFP)
B
CD31
PDGFRβ-GFP
NRP1
Arteriole
Ear skin
Back skin
50 µm
Arteriole
**
Perivascular NRP1 levels normalized to vascular NRP1
1.0
0.8
0.6
0.4
0.2
0.0
Ear skin
Back skin
C
Capillary
Ear skin
Back skin
Capillary
p=0.0841
Perivascular NRP1 levels normalized to vascular NRP1
1.0
0.8
0.6
0.4
0.2
0.0
Ear skin
Back skin
D
Venule
Ear skin
Back skin
Venule
***
Perivascular NRP1 levels normalized to vascular NRP1
1.0
0.8
0.6
0.4
0.2
0.0
Ear skin
Back skin

Figure 4

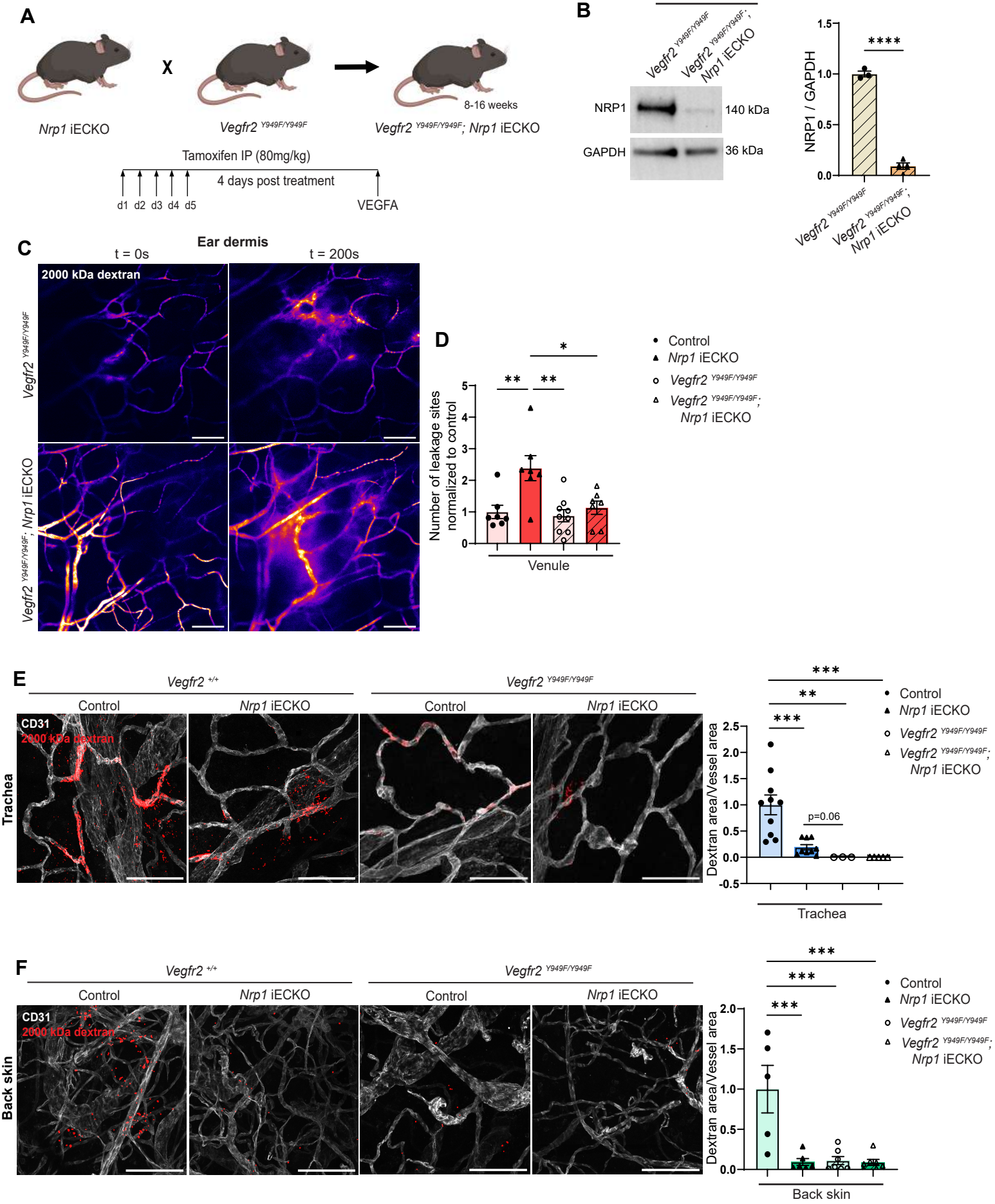
A
Nrp1 iECKO
X
Vegfr2 Y949F/Y949F
8-16 weeks
Vegfr2 Y949F/Y949F; Nrp1 iECKO
Tamoxifen IP (80mg/kg)
4 days post treatment
d1 d2 d3 d4 d5
VEGFA
B
Lung lysates
Vegfr2 Y949F/Y949F
Vegfr2 Y949F/Y949F; Nrp1 iECKO
NRP1
140 kDa
GAPDH
36 kDa
NRP1 / GAPDH
****
C
Ear dermis
t = 0s
t = 200s
2000 kDa dextran
Vegfr2 Y949F/Y949F
Vegfr2 Y949F/Y949F; Nrp1 iECKO
D
Number of leakage sites normalized to control
Venule
Control
Nrp1 iECKO
Vegfr2 Y949F/Y949F
Vegfr2 Y949F/Y949F; Nrp1 iECKO
E
Vegfr2 +/+
Vegfr2 Y949F/Y949F
Control
Nrp1 iECKO
Trachea
CD31
2000 kDa dextran
Dextran area/Vessel area
p=0.06
F
Back skin

Figure 5

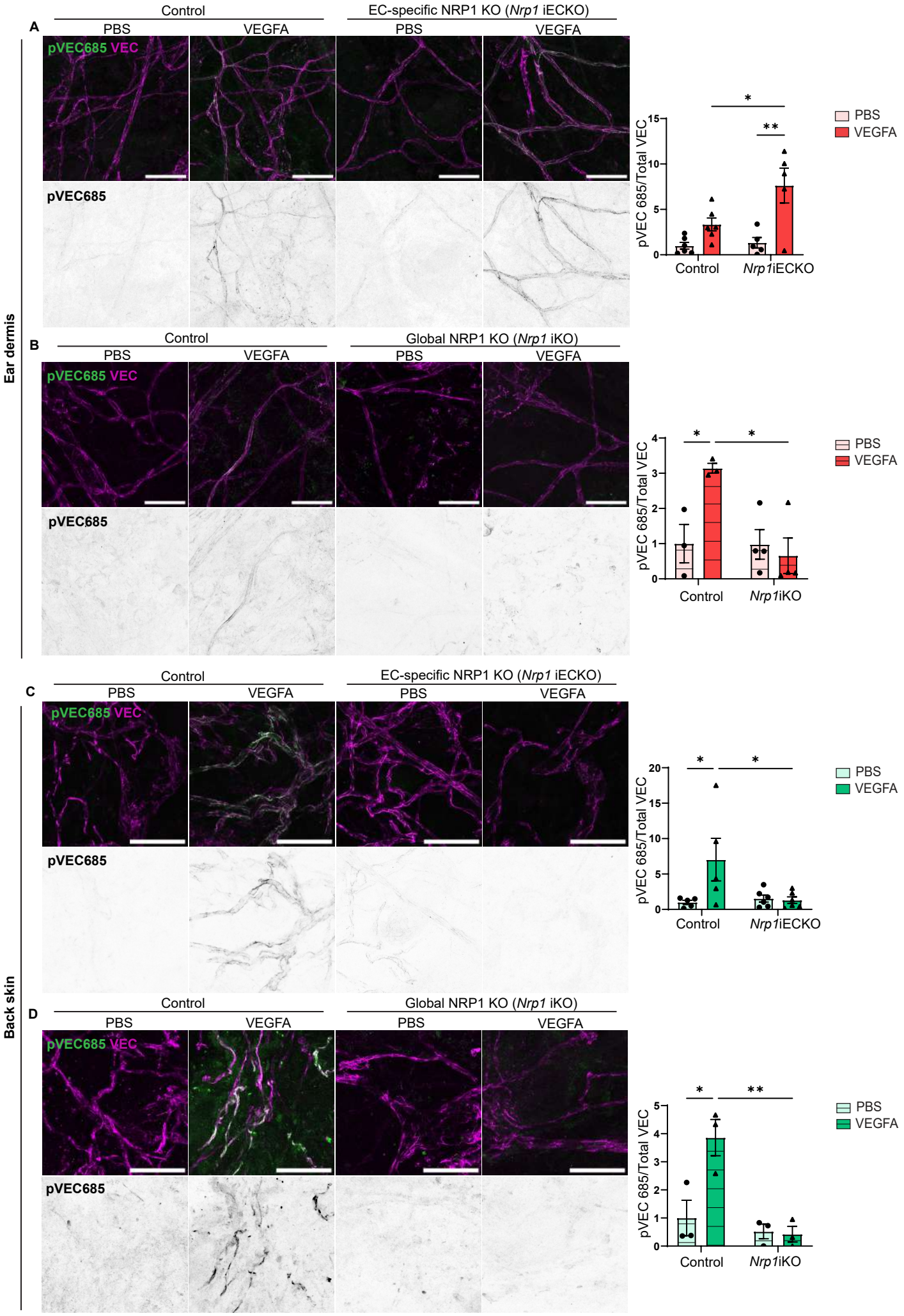
A
Control
EC-specific NRP1 KO (Nrp1 iECKO)
PBS
VEGFA
PBS
VEGFA
pVEC685 VEC
pVEC685
pVEC 685/Total VEC
Control
Nrp1iECKO
PBS
VEGFA
B
Control
Global NRP1 KO (Nrp1 iKO)
PBS
VEGFA
PBS
VEGFA
pVEC685 VEC
pVEC685
pVEC 685/Total VEC
Control
Nrp1iKO
PBS
VEGFA
Ear dermis
C
Control
EC-specific NRP1 KO (Nrp1 iECKO)
PBS
VEGFA
PBS
VEGFA
pVEC685 VEC
pVEC685
pVEC 685/Total VEC
Control
Nrp1iECKO
PBS
VEGFA
D
Control
Global NRP1 KO (Nrp1 iKO)
PBS
VEGFA
PBS
VEGFA
pVEC685 VEC
pVEC685
pVEC 685/Total VEC
Control
Nrp1iKO
PBS
VEGFA
Back skin

Figure 6

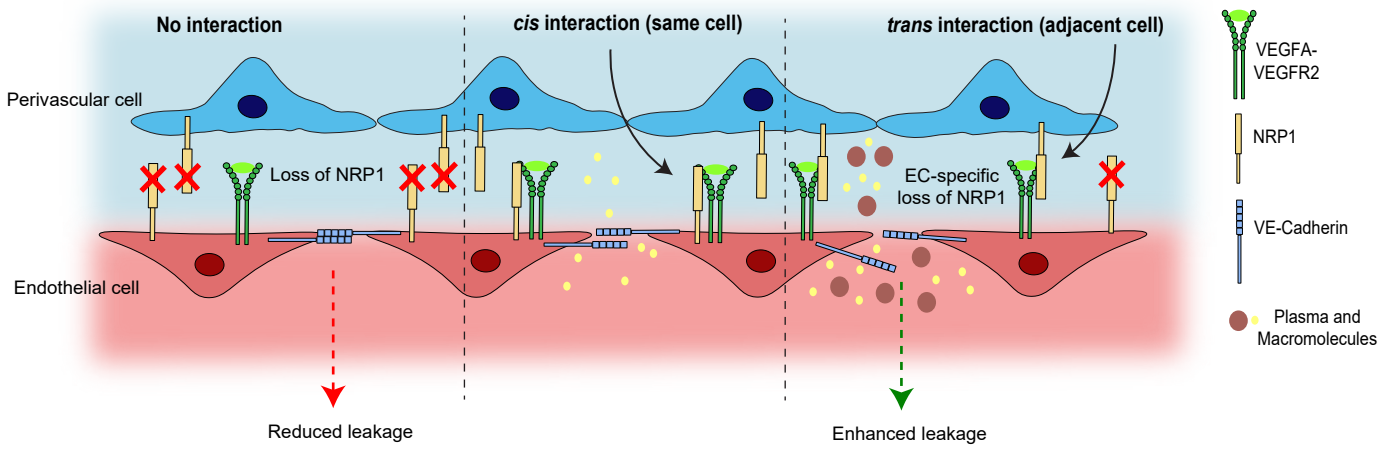
No interaction
cis interaction (same cell)
trans interaction (adjacent cell)
Perivascular cell
Loss of NRP1
EC-specific
loss of NRP1
Endothelial cell
Reduced leakage
Enhanced leakage
VEGFA-
VEGFR2
NRP1
VE-Cadherin
Plasma and
Macromolecules

Supp fig 1

A NRP1 expression in ear dermis

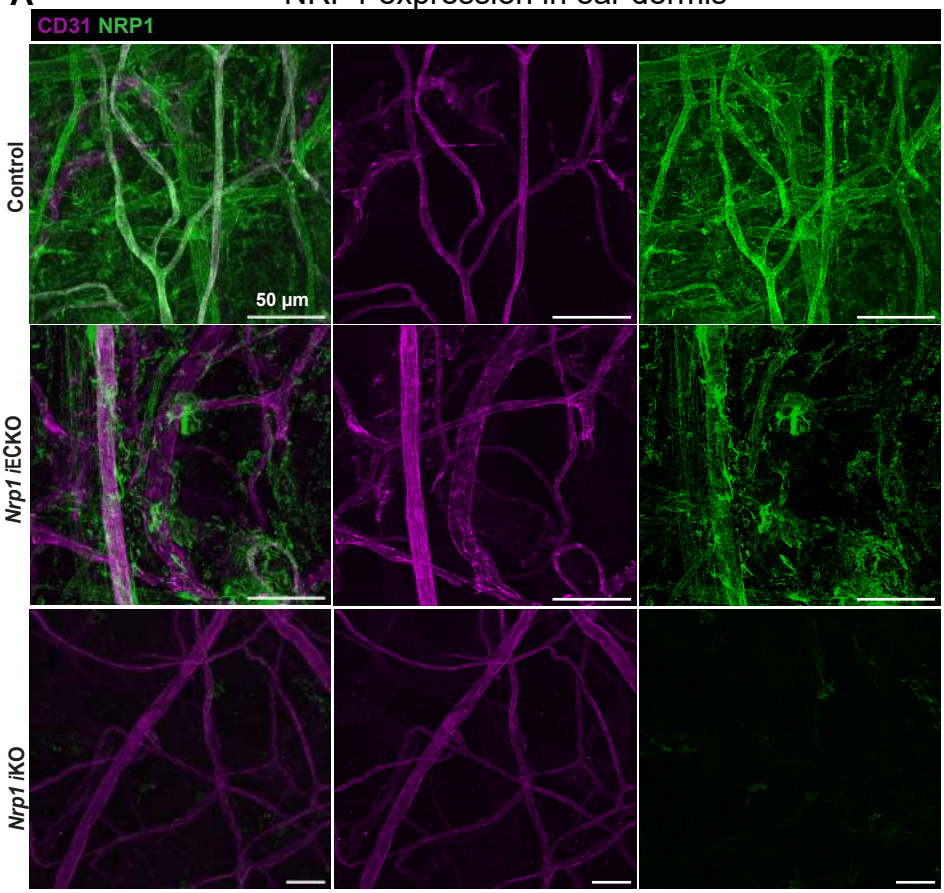

B NRP1 expression in back skin

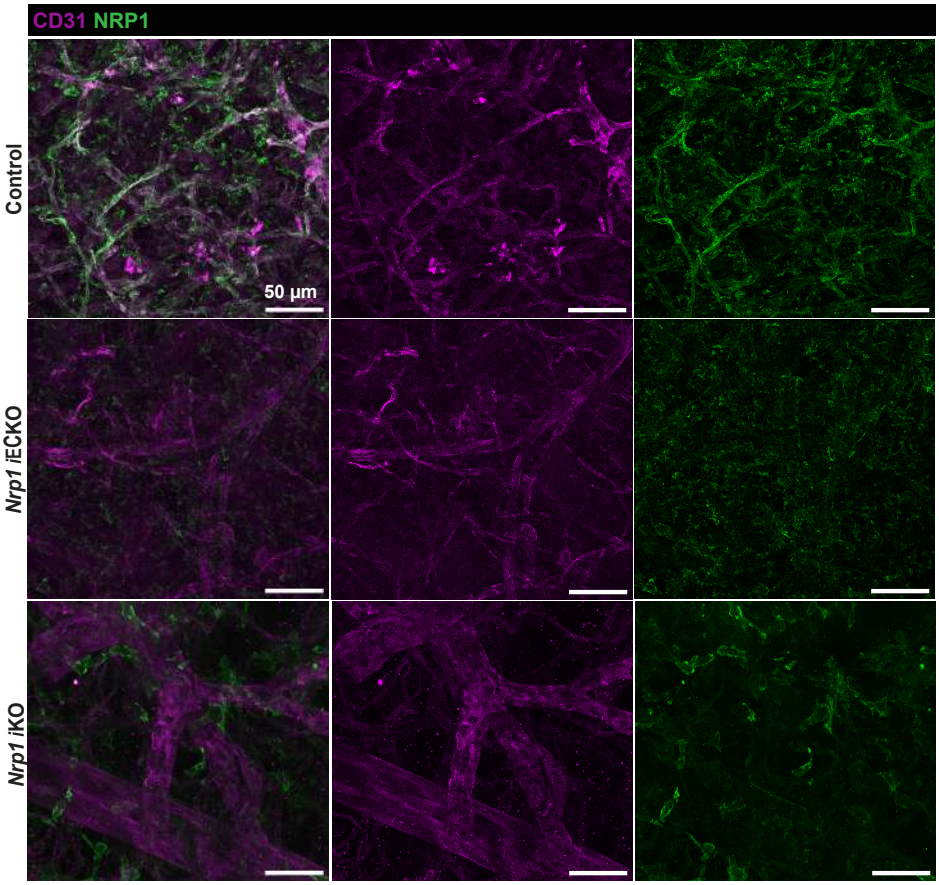

Supp fig 2

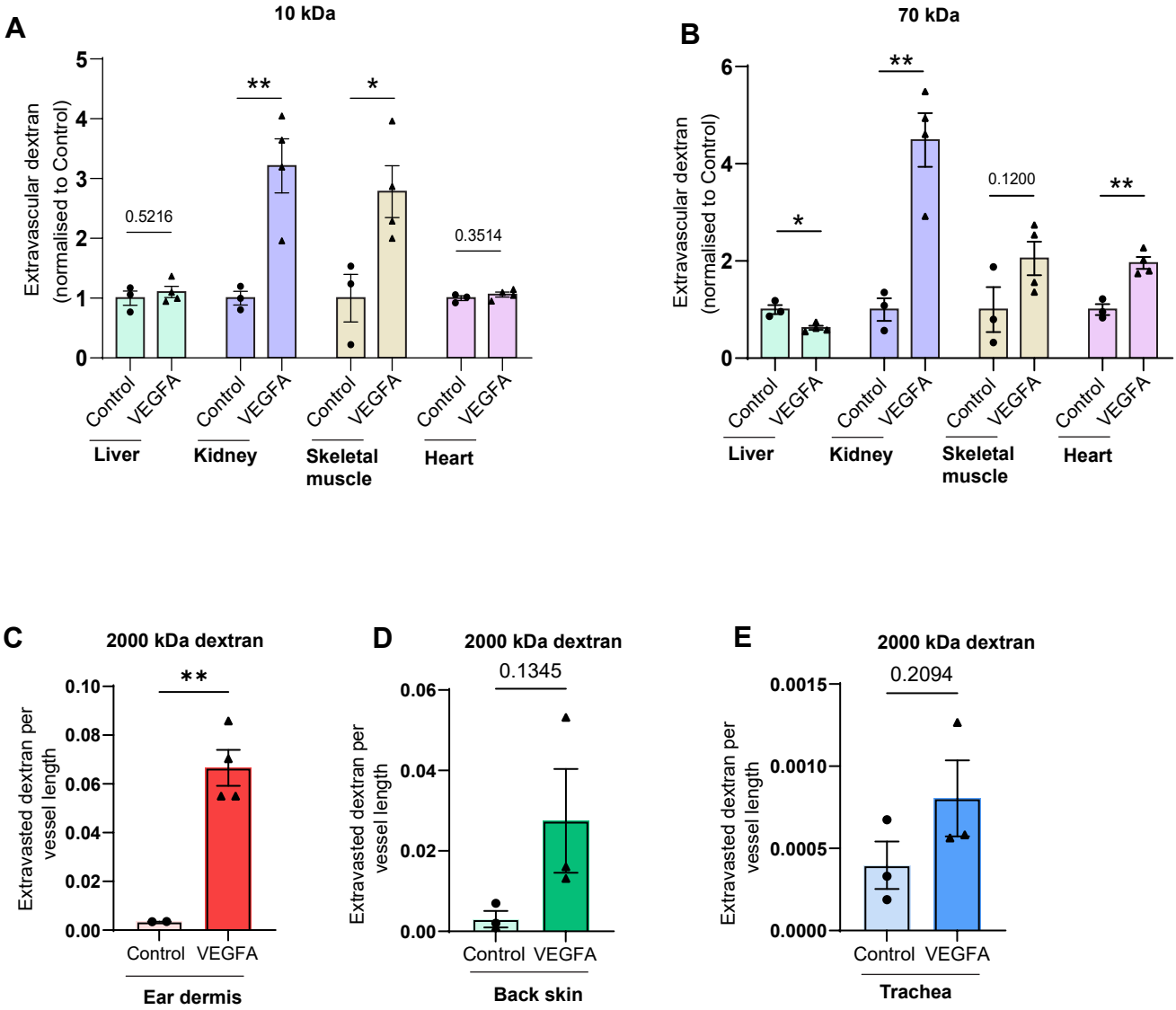
A
10 kDa
Extravascular dextran (normalised to Control)
0
1
2
3
4
5
0.5216
**
*
0.3514
Control
VEGFA
Liver
Kidney
Skeletal muscle
Heart
B
70 kDa
Extravascular dextran (normalised to Control)
0
2
4
6
*
**
0.1200
**
Control
VEGFA
Liver
Kidney
Skeletal muscle
Heart
C
2000 kDa dextran
Extravasted dextran per vessel length
0.00
0.02
0.04
0.06
0.08
0.10
**
Control
VEGFA
Ear dermis
D
2000 kDa dextran
Extravasted dextran per vessel length
0.00
0.02
0.04
0.06
0.1345
Control
VEGFA
Back skin
E
2000 kDa dextran
Extravasted dextran per vessel length
0.0000
0.0005
0.0010
0.0015
0.2094
Control
VEGFA
Trachea

Supp fig 3

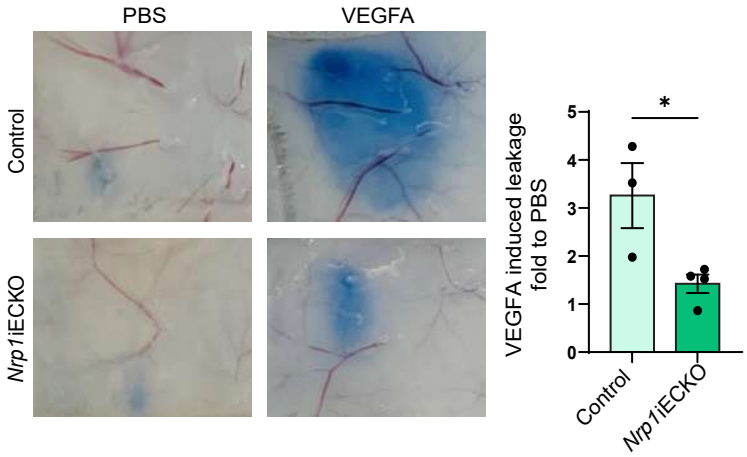
PBS
VEGFA
Control
Nrp1iECKO
VEGFA induced leakage fold to PBS
*
0
1
2
3
4
5
Control
Nrp1iECKO

Supp fig 4

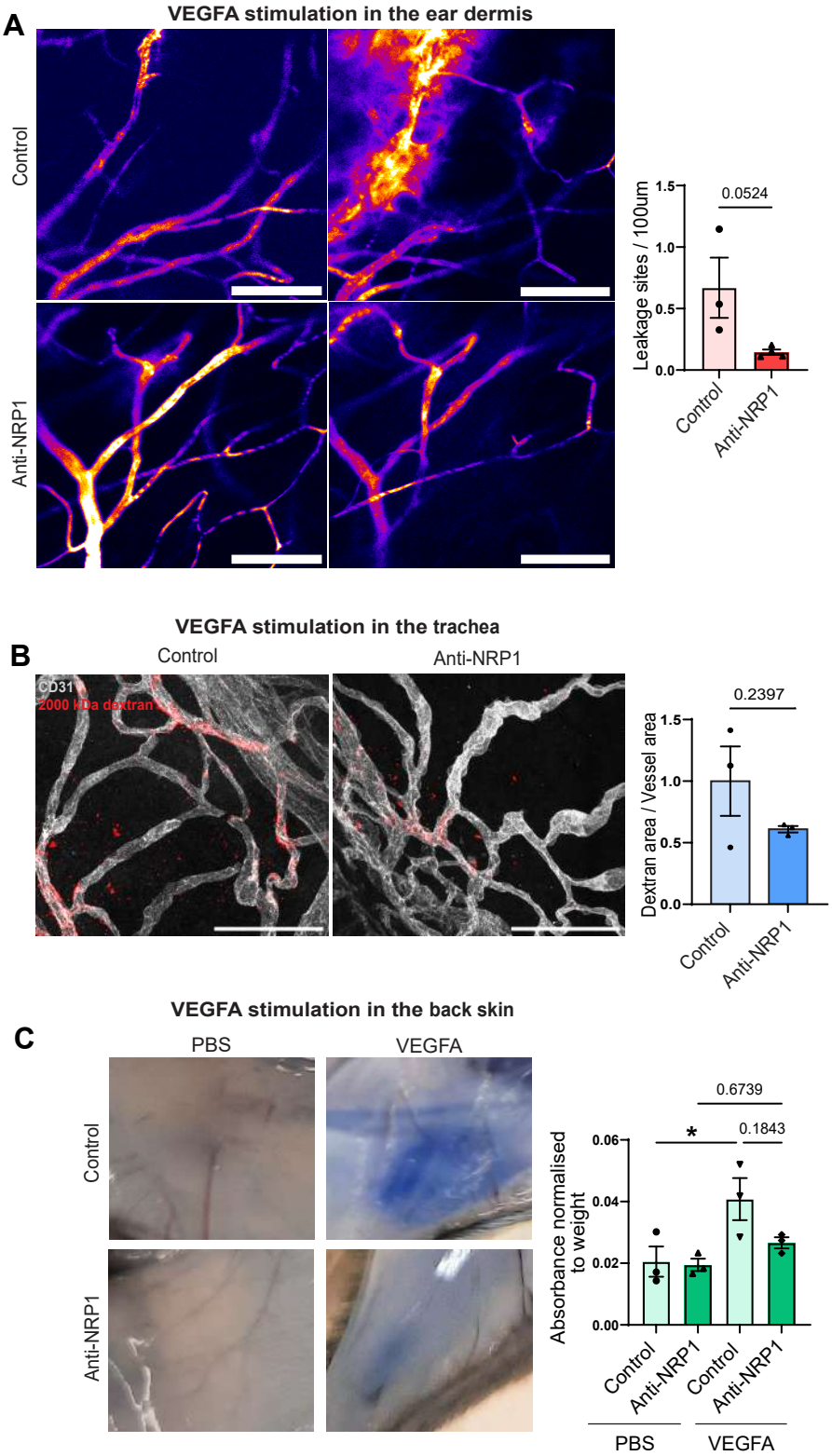
A
VEGFA stimulation in the ear dermis
Control
Anti-NRP1
Leakage sites / 100um
1.5
1.0
0.5
0.0
0.0524
Control
Anti-NRP1
B
VEGFA stimulation in the trachea
Control
Anti-NRP1
CD31
2000 kDa dextran
Dextran area / Vessel area
1.5
1.0
0.5
0.0
0.2397
Control
Anti-NRP1
C
VEGFA stimulation in the back skin
PBS
VEGFA
Control
Anti-NRP1
Absorbance normalised to weight
0.06
0.04
0.02
0.00
0.6739
*
0.1843
Control
Anti-NRP1
Control
Anti-NRP1
PBS
VEGFA

Supp fig 5

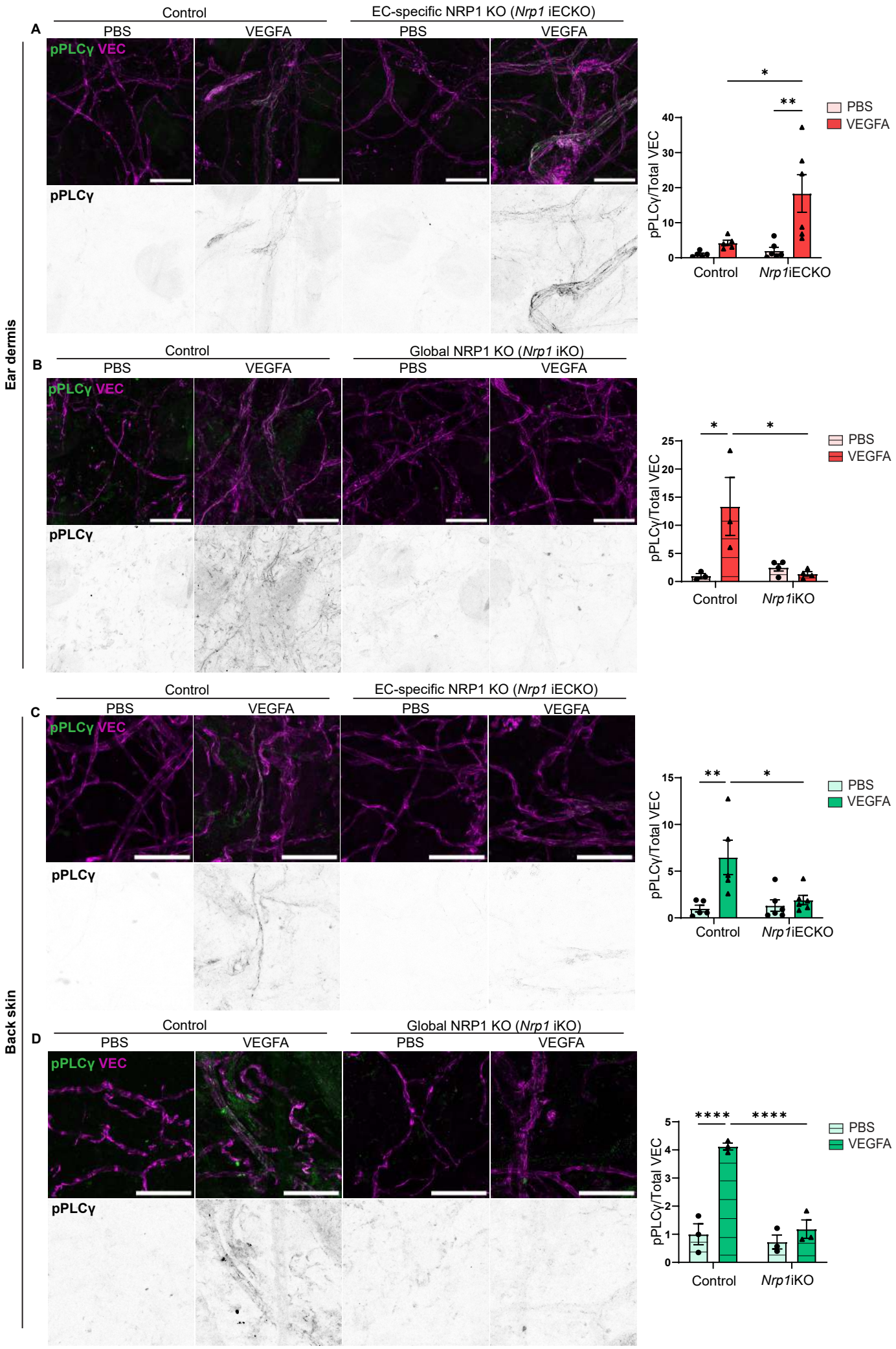
Ear dermis
A
Control
EC-specific NRP1 KO (Nrp1 iECKO)
PBS
VEGFA
PBS
VEGFA
pPLCγ VEC
pPLCγ
pPLCγ/Total VEC
Control
Nrp1iECKO
PBS
VEGFA
B
Control
Global NRP1 KO (Nrp1 iKO)
PBS
VEGFA
PBS
VEGFA
pPLCγ VEC
pPLCγ
pPLCγ/Total VEC
Control
Nrp1iKO
PBS
VEGFA
Back skin
C
Control
EC-specific NRP1 KO (Nrp1 iECKO)
PBS
VEGFA
PBS
VEGFA
pPLCγ VEC
pPLCγ
pPLCγ/Total VEC
Control
Nrp1iECKO
PBS
VEGFA
D
Control
Global NRP1 KO (Nrp1 iKO)
PBS
VEGFA
PBS
VEGFA
pPLCγ VEC
pPLCγ
pPLCγ/Total VEC
Control
Nrp1iKO
PBS
VEGFA